Age-effects on Resting State Dynamics of Cortical Networks

Thesis submitted in partial fulfillment
of the requirements for the degree of

Master of Science by Research
in
Computer Science

by

Shruti Naik
201407630
naik.shruti@research.iiit.ac.in

Cognative Science Lab
International Institute of Information Technology
Hyderabad - 500 032, INDIA
July 2017

International Institute of Information Technology
Hyderabad, India

CERTIFICATE OF AUTHORSHIP

I, Shruti Naik, declare that the thesis, titled "Age-effects on Resting State Dynamics of Cortical Networks", and the work presented herein are my own. I confirm that this work was done wholly or mainly while in candidature for a research degree at IIIT-Hyderabad.

Date	Signature of the Candidate

International Institute of Information Technology
Hyderabad, India

CERTIFICATE

It is certified that the work contained in this thesis, titled "Age Effects on Resting State Dynamics of Cortical Networks" by Shruti Naik, has been carried out under my supervision and is not submitted elsewhere for a degree.

Date

Adviser: Prof. Bapi Raju Surampudi

To

Amish Sir

(Without whom I would not have developed scientific thinking.)

Acknowledgements

I am grateful to Prof. Bapi Raju for interesting me into the fascinating field of Cognitive Neuroscience and for the freedom he endowed in selecting this research topic. I am also thankful for all the stimulating discussions with him and Prof. Dipanjan Roy that helped me remain focused while exploring uncharted areas of research. I was fortunate to receive a detailed review of my work from Prof. Arpan Banerjee and Prof. Gustavo Deco. I extend my gratitude towards Dr. Suvarna Alladi for our conversations with regards to aging-related early decline, mild cognitive impairment and clinical importance of my work. I am grateful to the TATA imaging project team at Nizam's Institute of Medical Sciences (NIMS), Hyderabad for their support in learning neuroimaging data acquisition and preprocessing methods. I thank Raghav Mehta and Anirudh Vatikonda for helping me surpass the caveats of data preprocessing. A special mention goes to Mr. P L Murthy for helping me with any administrative work with ever smiling face. Constructive philosophical discourse with Pramod Kaushik, Gautam Malu and Snehil Joshi on wide-ranging topics including Brain, Mind, Machines and Consciousness has helped me realize the importance of intuition and childlike curiosity in the radical empiricist research world. I am grateful to all the lab members with whom I have had interesting discussions about work and life which kept me motivated. Finally, I am lucky to have a supportive family without whom this endeavor would not have been possible.

This study was funded by IIIT Hyderabad. Part of the study was also funded by A.B. Ramalingaswami fellowship (BT/RLF/Re-entry/31/2011) and Innovative Young Bio-technologist Award (IYBA) to DR (BT/07/IYBA/2013) and from Department of Biotechnology, Ministry of Science and Technology, Government of India to AB. GD is supported by the ERC Advanced Grant: DYSTRUCTURE (n. 295129), by the Spanish Research Project PSI2013-42091-P. and funding from the European Union Seventh Framework Programme (FP7-ICT Human Brain Project (grant no. 60402))

I would like to acknowledge department of Neurology, Charité, Charitéplatz, Berlin for making the valuable data available for this study. I was greatly benefited from the preprocessed data available by the Nathan Kline Institute, Rockland and by the open-science initiative- UMCD Human Connectome Project which is effortlessly working towards the noble goal of easy data-sharing.

Abstract

The brain during healthy aging exhibits gradual deterioration of structure but maintains comparatively high level of cognitive ability. These structural changes are often accompanied by reorganization of functional brain networks. Existing neurocognitive theories of aging have argued that such changes are either beneficial or detrimental. Despite numerous empirical investigations, the field lacks a coherent account of the dynamic processes that occur over our lifespan. Taking advantage of the recent developments in whole-brain computational modeling approaches, we hypothesize that the continuous process of aging can be explained by the concepts of metastability – a theoretical framework that gives a systematic account of the variability of the brain. This hypothesis can bridge the gap between existing theories and the empirical findings on age-related changes.

This thesis majorly contributed in our understanding of the aging brain in three different ways: First, we analyzed the age-related changes in the complex network measures of structural and functional brain networks. The results from this study in accordance with other studies in the literature demonstrated that the structural and functional connectivity networks are affected differentially by age. This gave rise to the need for understanding the 'dynamics' of the resting state networks using more sophisticated measures.

Hence in the second study, we empirically investigated the variability of the phase-synchronization (i.e. metastability) patterns of the known resting state brain networks and found that these features can successfully classify the instances of healthy young, middle-aged and old subjects. These results for the first time in aging literature empirically confirmed the role of metastability in understanding aging effects.

In the third study, we attempted to give a computational account of these empirical results. We carried out simulations of two whole-brain computational models– reduced dynamic mean field model and Kuramoto model. Each of these models is generative and bottom-up in nature. That is, in both the cases we attempt to simulate resting state fMRI signals (and in turn functional connectivity networks) by modeling the population neural activity at each node of the structural connectivity graph. Preliminary results from this study confirmed that healthy aging subtly 'shifts' the parameter-space in both the models. Moreover, metastability of the

simulated neural activity from Kuramoto Model showed similar trends seen in the empirical investigation of the fMRI (BOLD) signals. Our findings suggest that healthy aging alters the dynamical working point of the system, which in turn affects the metastability of various neural signals obtained at different scales.

In future, similar studies can be devised with improved measures of metastability and on larger and possibly longitudinal aging data sets. These results can be correlated with the behavioral scores to understand whether such shifts in dynamical working point facilitate or deteriorate the performance of the elderly.

Contents

List of Figures

List of Tables

Chapter 1

Introduction

1.1 Motivation

Healthy aging has always been associated with inevitable physical and behavioral deterioration. However, years of scientific scrutiny of this idea has revealed that age-related changes are not straightforward. While some cognitive functions such as numerical and verbal skills, vocabulary, emotion processing, and general knowledge about the world remain intact with age, other mental capabilities decline from middle age onward: these mainly include episodic memory (ability to recall a sequence of events as they occurred), processing speed, working memory, and executive control [11, 12, 13, 14]. The *in vivo* investigation of changes in healthy aging brain became viable after the advancement in Magnetic Resonance (MR) imaging techniques in the last three decades. Recently with the use of diffusion tensor imaging (DTI), tracking of long-range white matter micro-structures became feasible. On the other hand, functional magnetic resonance imaging (fMRI) helped in localization of various task-conditions and investigated the correlates of cognitive performance across age-groups. The reports from these studies remain ambiguous. On the one hand, there is notable structural decline across brain regions while on the other hand, the brain activity in those regions is often reported to *increase* in healthy older adults when they perform specific tasks. These empirical results have left the aging researchers debating whether the functional changes are beneficial or detrimental in terms of task performance. Despite adequate experimental evidence in support of both the hypotheses, aging studies lack a coherent view on how age-related structural and functional changes can be explained in a single theoretical framework.

With the exception of a few recent ones, most studies on aging in the last decade targeted a select few regions of the brain to find a bio-marker for healthy aging. However, *no brain region is an island* and hence it is important to understand how the *structural connections* and functional interactions change across age-groups. Many sincere attempts have been made in

this direction by a select few research groups [2, 5, 15]. This thesis aims to outline the strengths and limitation of these efforts. It further extends the scope of the domain by introducing the notion of age-related changes in the *dynamics* of the brain. We argue that one must consider the dynamic, *connectionist view* of the brain in order to relate structural changes to functional changes occurring across lifespan [16].

The dynamics of the brain is being studied extensively in both empirical and computational neuroscience to understand how the baseline activity of brain (activity at rest- in absence of any stimulus) is generated [17, 18] . This spontaneous brain activity as measured by the functional MRI is not random but is spatio-temporally organized. This, so called, 'resting state functional organization' is closely related to, but not limited by the underlying structural connections [19]. Many theoretical approaches now point towards the existence of rich dynamics that might play a role along with the structure of the brain in generating rich spatio-temporal functional patterns [20, 21]. On the other hand, empirical studies have found that the time-variable resting state connectivity patterns is widely affected during various clinical conditions [22, 23] . The fluctuation of these resting-state patterns in time can therefore be a valuable measure to understand age-related changes in the dynamics of the brain. Major part of this thesis explores novel measures for quantifying the time-variability in the resting state networks for the aging dataset. Further, **whole-brain computational modeling** approaches have been employed for computational characterization of this variability and quantifying the change in the dynamics across subjects of different ages. In the next sections, we go on to explain core concepts used in this thesis.

1.2 Resting State Activity

When a person is lying down with her/his eyes closed or fixated on one point, (s)he is considered to be at rest. In this state, (s)he is awake and still able to attend to an unexpected external stimuli (e.g., a sudden sound) but is not performing any cognitively demanding task in particular. The spontaneous activity of the brain in this state is known as the **resting state activity** or the **default mode activity**. This activity is spatially organized across brain regions [24] and involves the exact same brain regions that are also involved in the higher-level cognitive functions such as mind wandering, self-related thoughts or remembering the past events [25, 26, 27]. However, this baseline activity is also present in anesthetized monkeys and rats [28, 29] and during other vigilance states such as light sleep [30]. These evidences suggest more preliminary cause of this default mode activation e.g., this baseline activity might emerge from the structurally and dynamically shaped background noise.

The resting state activity of a few brain structures highly temporally coincides with each other. These regions form a correlational network pattern known as the 'default mode net-

work (DMN)' [31]. The activity of DMN regions subsides during task condition and hence the DMN is also known as *task-negative* network. Contrary to DMN, there are other regions which are highly co-activated during the cognitive processes such as executive function, attention and sensory processing during the task conditions. Since these regions co-activate during the rest and task alike, they are known as the *task-positive* networks. Together with the DMN, these networks are collectively known as the resting state networks (RSN) [32]. Apart from the DMN, the known resting state networks include but are not limited to Ventral and Dorsal Attention Network, Cingulo-opercular Network, Fronto-Parietal Control Network, Somatosensory Network, Limbic Network etc.

These co-activation patterns of the resting brain are robust across participants [33] and across trials in the same participant [34]. Due to its high reliability and reproducibility, RSNs are considered the so-called 'functional organization' of the brain. This functional organization is known to change during learning [35], maturation [36], vigilance states and in many clinical conditions (See [37] for review). Despite robust inter-subject patterns across RSNs, consistent inter-individual variability exists and is highly determined by the subject's age [38]. For example, the DMN co-activation (or connectivity) is consistently shown to reduce with advanced aging [39, 40]. Moreover, this reduced DMN connectivity is shown to correlate with the poorer performance in older adults [41, 42]. Most of the studies that investigated age-effects on the resting state activity focused on the DMN and ignored other RSNs. Very few studies that investigated other RSNs [43, 44] suggest a more complex interaction between connectivity changes and cognitive performance of the elderly. For example, reduced connectivity does not always result in poorer performance and increased connectivity between particular regions does not always mean better performance (Comprehensive review on these findings follow in the next chapter). These results emphasized the need for studying the age-related changes in resting state networks in an extensive detail.

A more recent approach based in the graph theory covers the *whole-brain* and considers the resting state connectivity between *all* pairs of brain regions and can provide a global picture. In the next section we discuss these approaches and how functional organization can be related to the structure of the brain.

1.3 Neuroimaging Techniques & Networks of the Brain

Human brain can be viewed as a complex network of spatially segregated, functionally specialized brain regions. According to a neuropsychological theory of 'global neuronal work-space', higher-order cognitive functions are not carried out by the single brain region but it emerges from the distributed processing across a large brain network [45]. This theory can now be in-

vestigated computationally (formally) by constructing structural and functional brain networks and analyzing their properties using concepts from graph theory.

In the next subsection, we first discuss the definition of the node (the basic unit of graph) in the context of brain networks and then discuss the two most common neuroimaging methods (rs-fMRI and DTI) that are used to define the edges of functional and structural connectivity graphs respectively.

1.3.1 Anatomical Parcellation & Nodes of Brain Graphs

A graph G = (V,E) is defined as a set of N nodes $\{V = V_i | i = 1...N\}$ and a set of edges given by an ordered node pair $E = \{(i,j)|i,j \in V\}$. To construct such a graph from neuroimaging data, one first needs to define the set of nodes V. The nodes of the brain graphs are typically the GM structures parcellated using predefined atlases. Size of network or number of nodes, N depends on the parcellation scheme used for dividing the brain's gray matter into valid cortical structures.

Typically, subject-specific structural T1-weighted MR images are registered to the predefined atlas for this purpose. An atlas is created by automatic or manual segmentation (and labeling) of the cytoarchitecturally valid GM regions on the T1 standard templates. The standard templates are derived after non-linear registration and averaging of T1 scans from many subjects. Some of the standard templates include MNI152 [46], ICBM452 [47], Indian Brain Atlas (IBA100) etc. See [48] for extensive details on brain templates and atlases. Various parcellation schemes are applied to investigate networks of different sizes. The highest resolution parcellation scheme for graph theoretic studies used till date is N=998 regions derived for the structural connectivity analysis by Hagmann *et al* [49]. For this, the GM region was segmented from the T1-images, 66 anatomical landmarks were found for each subject-specific GM images and each of these regions were further divided into smaller clusters such that each cluster covers exactly 1.5 cm^2 of the cortical surface (total N=998). Other parcellation schemes include N=90 regions using AAL atlas [50], which was obtained by automated anatomical labelling of the MNI template, Harvard-Oxford atlas having N=120 cortical regions [51], and Desikan-Killiany probabilistic atlas having N=68 cortical regions ([6]) etc.

A few functional networks studies considered defining nodes using the functional landmarks from the fMRI data. For example Independent Component Analysis (ICA) can be used to identify clusters of highly temporally correlated voxels (known as ICs) which are spatially independent from each other. Each of these ICs then represent a node in the network. Note that unlike anatomical definition of nodes, IC defined nodes are not contiguous in space and cannot be used for the white-matter fiber tractography. Hence, such definition of nodes is not very common and is not suitable for the comparison of structural and functional brain networks. However, at least

two studies have tried to construct spatially constrained functional atlases that are spatially contiguous and are widely used for brain mapping. These include an atlas by Craddock *et al.* [52](N=200) and by Power *et al.* [53](N=264).

To investigate network properties at different scales, the lower resolution parcellations can further be up-sampled such that each region in this parcellation can be divided into fixed set of smaller regions. However, due to high computational costs involved in doing so, most studies have limited their investigation to only one of the parcellation schemes.

1.3.2 Diffusion Tensor Imaging (DTI) & Structural Brain Networks

The structural brain networks can be viewed as the mathematical representation of the brain's wiring diagram. The white-matter tissue of the brain essentially contains long-range axon fiber bundles that connect majority of the gray matter regions. These large scale connections constrain the communication between the gray matter regions to some extent and hence, studying the network of these fibers or the wiring diagram is important. In humans, the direction and number of white-matter fiber bundles or streamlines can be indirectly estimated *in vivo* using diffusion tensor imaging (DTI) and efficient diffusion tractography algorithms [54]. DTI imaging uses an MR sequence sensitive to the diffusion of the water molecules. If the water molecule is closer to a white-matter streamline, the diffusion will be anisotropic in the direction of the fiber and hence the fractional anisotropy (FA) of the DTI signal will be higher in the direction of the fiber. Hence, post-processing tractography algorithms can be used to iteratively estimate the diffusion direction (or FA values) in each voxel that can finally estimate white-matter fibre trajectories in all three dimensions. Each of the nodes (as defined by the parcellation scheme) is used as the seed-region and all other nodes are considered to be target regions. The tractography algorithm is then run starting from each of the voxels in the seed region to estimate the streamlines of fibers. Various techniques can be used to stop the streamline estimation when it hits the target region [55, 7].

Three types of connectivity measures can be estimated between nodes i and j at the end of this computationally costly task:

- Number of white matter streamlines starting from the voxels in node i and ending in the voxels in node j.
- Average strength of white-matter fibers connecting nodes i and j in terms of mean FA values or mean diffusivity (MD) values.
- Distance between regions i and j in terms of average number of voxels traversed by the white-matter streamlines that start in voxels of region i and end in voxels of region j.

An $N \times N$ structural connectivity matrix (SC) is then constructed such that each element (i, j) represents any of the connectivity measures describes above. If the average connectivity measures are considered, the SC matrix will be symmetric, representing undirected structural network. However, in some cases, the connectivity measure is normalized by the number of voxels in the target region. In those cases, SC can be asymmetric matrix representing a directed anatomical network. Throughout this thesis, we will consider undirected weighted structural connectivity.

1.3.3 Functional Imaging & Functional Brain Networks

Functional brain networks have been constructed using many modalities including Electroencephalography (EEG), Magnetoencephalography (MEG) and functional Magnetic Resonance Imaging (fMRI) data. Due to higher spatial resolution of fMRI, it is the most used modality for constructing functional brain networks till date.

fMRI is an *in vivo* (non-invasive) and indirect measure of neural activity. It relies on the coupling between the neural activity and cerebral blood flow. When the local neural activity increases in some region, cerebral blood flow increases in this region which in turn decreases the deoxygenated hemoglobin. The oxygenated hemoglobin (Hb) is diamagnetic (repulsing the magnetic field) while the deoxygenated hemoglobin (d-Hb) is paramagnetic (weakly attracted to the applied magnetic field). In presence of external magnetic field, the decrease in d-Hb translates into a subtle increase in the local MR signal to noise ratio, which is known as Blood Oxygen Level Dependent (BOLD) signal. Hence, BOLD signal can be used as an indirect measure to capture underlying neural activity. With current techniques, we are able to obtain $1mm^3$ of resolution spatially and 1 s temporally.

The most common resting state networks were identified as the correlation between very low-frequency fluctuations (0.01-0.08 Hz) of the BOLD signals. Therefore to estimate the functional brain networks, the low-pass filtered (typically $<$0.08Hz) BOLD signals are used. Many statistical measures were proposed to estimate the strength of interaction e.g. correlation, coherence, mutual information or co-variance. The most widely used method to calculate this functional connectivity (FC) consists estimating the pairwise linear (Pearson) correlation coefficient between BOLD signals. If we consider pairwise Pearson correlation between time-series of each of the N nodes of the brain (as defined in the previous subsection), an $N \times N$ symmetric weighted adjacency matrix $\mathbf{W}$ can be obtained where each element $W(i, j)$ represents the weight of an edge between nodes i and j. A weighted, undirected graph represented by this matrix can be visualized as in fig. 1.1. If the node definition is based on the functional ICs, then the IC time-series can be used for generating a similar network.

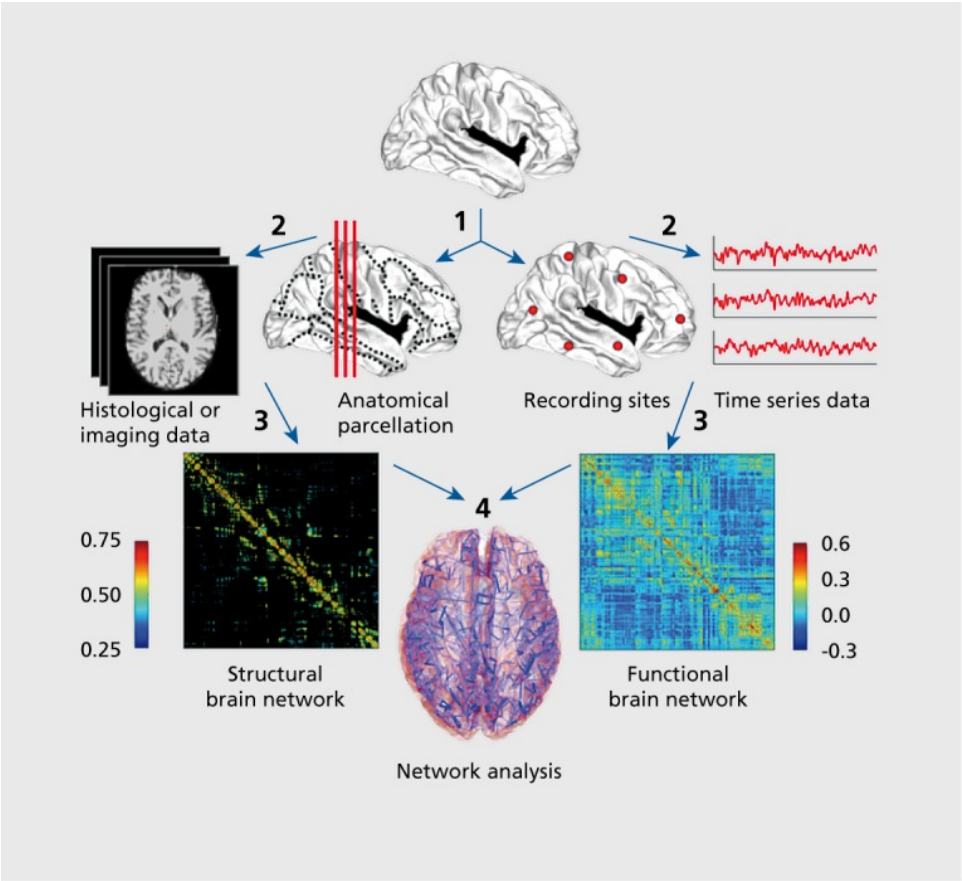

Figure 1.1: Construction of brain networks using neuroimaging data. The steps involved in this process are as follows: 1. Definition of network nodes by structural or functional parcellation; 2. Definition of network edges, either by estimating white-matter fiber tracts using diffusion tractography (left), or by estimating statistical dependencies among regional time-series signals (right); 3. Constructing weighted/binary adjacency matrix; 4. Analysis of global and nodal network features. Figure adapted from [1].

SC-FC relationship

The structural and functional networks obtained from neuroimaging data exhibit similar properties as that of complex networks– small-worldness, modularity, power law degree distribution etc. However, there are many striking differences among these networks. E.g., the structural networks (SC) are very sparse while the functional networks (FC) are dense. In other words, many nodes have highly correlated activation even without the existence of anatomical connectivity between them, suggesting an indirect communication route. Nonetheless, higher SC between node-pairs also predict higher FC between them. This led to a hypothesis that FC network is shaped by the SC network but cannot be entirely determined by the SC. In attempt to fully understand SC-FC relationships, whole-brain computational models are devised and the dynamics at the local nodes due to population neural firing is considered. Since aging affects SC and FC in different ways, it is important to study whole-brain computational models. In the next section we introduce these models.

1.4 Whole-brain Computational Models

Human brain operates at many different spatio-temporal scales. For example, neural signals can be captured from many spatio-temporal scales- spikes from single neuron recording sites (<ms), firing rate from population of neurons (<ms), Local field potential at scalp (approx. 0.1 s) and finally, very slow, BOLD signals using fMRI (approx. seconds). Therefore, while simulating the brain activity it is important to decide at which scale one would like to investigate the brain dynamics. Whole-brain computational models are designed to balance the trade-off between high biological realism and complexity to capture the most relevant dynamic mechanisms of the brain *in vivo*. This balance is not trivial given the astronomical number of neurons and the underspecified connectivity at the neural level. Hence, the most successful whole-brain computational models have taken their lead from statistical physics where it has been shown that macroscopic physical systems obey laws that are independent of their mesoscopic constituents. Indeed, the emergent collective macroscopic behavior of the brain models has been shown to depend only weakly on individual neuron behavior [56]. Thus, these models typically use mesoscopic top-down approximations of the dynamics at the local brain area networks, to simulate the macroscopic dynamics at whole-brain cortical networks. The simplest models use basic neural mass or mean-field models to capture changes in the mean firing rate, while the most advanced models use a dynamic mean field model derived from a reduction of a detailed spiking neuron model ([57] and references therein for review). Furthermore, the temporal dynamics of the local brain areas in these models can be chosen to be either asynchronous (spiking models or their respective mean-field reduction) [58, 18, 19] or oscillatory [59, 60, 61]. Recently, evidence has emerged for a promising version using for each brain area a local dynamical model given

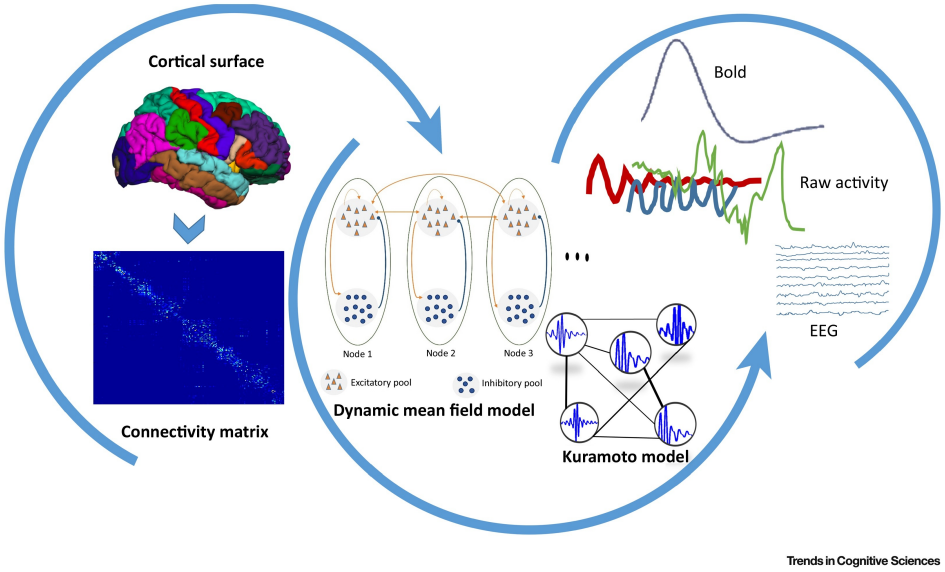

Figure 1.2: Typical Work-flow of Modeling Macroscale Brain Activity. The cortical surface template defines the parcellation. Diffusion tractography defines the connectivity matrix depending on the number of fibers or strength of diffusion. Each network node is modeled as a neural population having characteristic dynamics and interactions with other nodes. Forward models are used on the resulting network dynamics to generate potentials such as BOLD fMRI, or EEG signals.

by a normal form of bifurcation (e.g., a super-critical Hopf bifurcation). These models can describe the transition from noise to oscillations, and this captures importantly the richness and oscillations present in the temporal dynamics of the EEG [62] or BOLD data [63](Figure 1.2). Each of the above-described models reveals that the spatiotemporal patterns of spontaneous activity emerge when the system is sub-critical. For attractor networks, this means that a few regions show high activity and the rest are in a low-activity regime. For oscillators, this means that oscillations between a few regions are synchronized while the rest are asynchronous. Thus, the system of whole-brain complex network teeters between various stable states (multistability in the case of attractors) or dwells in a state other than the stable state (metastability in the case of oscillators and Hopf bifurcation), avoiding diseased states of complete order or complete disorder. Noise plays an important role and allows fluctuations between different stable states. This whole-brain computational modeling approach may provide an understanding of the fundamental mechanisms of the nonlinear structure-function relationship of the brain in aging.

1.5 Metastability in the Brain

As we have seen in the previous sections, brain at rest is not in a steady state. Neural ensembles in the brain oscillate at different frequencies during rest, transiently synchronizing and

desynchronizing with each other. This phenomena can be observed differently at different spatio-temporal scales (for e.g. in terms of resting state networks; if we consider large-scale cortical BOLD signals). This mechanism where the network elements (single neurons, neural population or brain regions) integrate with each other transiently and segregate in the next moment was loosely defined as the term 'metastability ' [10]. Metastability is hypothesized to be an important dynamic property of the neural signals by which the exploration of many different 'functional configurations' are possible even when the structure of the brain remains relatively constant at shorter timescales [21]. Taking hint from this, we proposed that metastability can be an important bridge to understand the age-related structure-function changes.

Metastability can be defined more concretely in theoretical and empirical investigations depending on the context. For e.g., in the context of dynamical systems (and hence, in whole-brain computational models) 'the metastable regime' can be obtained when the system is sub-critical (i.e. close to the stable state solutions, but never approaching to that solution). As seen in the previous section, several whole-brain computational studies find that the best fit between empirical data and simulated results can also be obtained in the sub-critical regime. If these computational studies are valid, one should also empirically find the signature of metastability in various neural signals.

In the context of neuroimaging data, metastability can be observed as the temporal fluctuations of the functional connectivity among brain regions. However, since the FC fluctuation can only be studied in discrete states, it is also often called 'multistability'. (In the context of computational modeling however, these two terms have precisely different meanings. We will discuss these in chapter 6). Since the empirical investigation of metastability itself is a nascent field, currently there is no best definition of the metastability of resting state networks. In the next section however, we will summarize various efforts made in defining the signature of metastability from BOLD signals.

Since the age-related change in SC-FC dynamics occur at different spatio-temporal scales, we hypothesized that the metastability should play an important role in predicting age. To test this hypothesis empirically, we defined metastability as the standard deviation of the phase-synchrony of BOLD signals. We will discuss this approach and results in Chapter 5 in detail. We discuss computational counterpart of this in chapter 6.

1.6 Contribution

In summary, the following are the main contributions of this thesis:

- *Hypothesis*: The idea that dynamics of the resting state networks is important to characterize aging has never been proposed before to the best of our knowledge. In this thesis

we systematically laid out theoretical, empirical, and computational framework to characterize the changes in the resting state dynamics of the aging brain. This framework provided proof of concept results and has opened up a new direction for more explorations in future.

- *Novel features for Age-group Classification*: We propose standard deviation in phase-synchronization of BOLD signals as a novel feature useful for age-group classification. This feature revealed many interesting results that could discriminate patterns of maturation (from young to middle-age) and aging (middle-age to old-age).

- *Personalized Whole-brain Computational Models*: We use personalized whole-brain computational models for the first time in aging studies to explore group differences. Although the results are preliminary, they gave interesting new direction to test many of the hypotheses that we speculate on a larger dataset or in the neurodegenerative clinical conditions.

1.7 Thesis Overview

The rest of the thesis is organized as follows: Chapter 2 narrates the theories of aging that exist in the domain of cognitive neuroscience and empirical results (related work) in this domain. Here we also describe how our approach to analyzing dynamics could potentially bridge the gap between some of these theories and empirical evidences. Chapter 3 describes the details of acquisition of neuroimaging dataset and the preprocessing steps involved to reach to the final connectivity matrices that were used for the data. Chapter 4 presents the network measures employed to evaluate the age-related differences in the structural and functional connectivity for our dataset. Since neuroimaging techniques often have reproducibility issues, it is important to first be assured that the standard graph-theoretic analyses can produce the well-known results about healthy aging and hence these analyses validated the dataset as well as the distribution of subjects in age-groups. Chapter 5 reports various methods for characterizing synchrony and metastability from the empirical data, application of the method of Linear Discriminant Analysis and interesting results from this analysis. Chapter 6 illustrates the two whole-brain models used for computationally validating the empirical results: Reduced dynamic mean field model and Kuramoto Model. This chapter also investigates the parameter exploration for the single-dimensional mean field model and two-dimensional Kuramoto model and how they can be used in future for more sophisticated analysis of metastability differences with age. Finally, Chapter 7 concludes the thesis and gives future directions.

Chapter 2

Neurocognitive Theories of Aging

In this Chapter we describe the extant neurocognitive theories of aging and the empirical results in this domain. In the end, we propose a way of bridging the gap between some of these theories and empirical evidences using measures from dynamical systems theory.

2.1 Dedifferentiation or Compensation?

Changes in the structure-function-cognition relationship with age are poorly understood in the literature. While some regions such as the prefrontal cortex show enhanced activation during task-performance, other regions exhibit suppressed activity. Compensation related utilization of neural circuit hypothesis (CRUNCH) proposes that over-activation is a common response across all age groups when cognitive demand is high, either due to task difficulty or structural impairment [64]. The hemispheric asymmetry reduction in older adults (HAROLD) theory makes similar observations but emphasizes the over-activity exhibited by task-unrelated contralateral brain regions in high-task demand condition [65]. Moreover, enhanced activation of the anterior prefrontal cortex co-exists with decreased activity of the posterior regions in the high-performing elderly. This led to the theory of 'Posterior to Anterior Shift in Ageing' (PASA) suggesting that older adults rely on the anterior frontal regions to compensate for the aberrant functional specificity of the posterior regions [66]. Increased activation of the anterior frontal areas during successful trials also correlates with decreased white-matter integrity of these regions and leads to the 'less wiring more firing' hypothesis [67]. Alternate explanation for the hyperactivity can either stem from the inability to selectively inhibit response with increasing age, caused possibly due to decreased efficiency of the networks involving the candidate regions or the increase of noise in the intrinsic dynamics of these regions. This process of dedifferentiation has been observed most directly in terms of decreasing modularity of functional networks with age [68] suggesting that functional specificity of the resting state networks declines with age. For

example, increased between-network connectivity of the fronto-parietal control network (FPCN) predicts reduced within-network connectivity of the default mode network (DMN), suggesting that FPCN might play an important role in coping with the age-related differences in other networks [69]. Further studies have observed that degree of suppression of the default mode activity becomes attenuated with increase in task demand [70]. Default (DMN) to executive coupling hypothesis of aging (DECHA) supported this view and reported that the elderly subjects showing reduced suppression of activity in the DMN fail to modulate the bilateral prefrontal cortex (DLPFC) in case of tasks demanding higher executive control [70].

In general, networks supporting primary functions are maintained till very late in life while others supporting more complex behaviour seem to become less efficient with age. 'Last in first out' theory suggests that networks involving regions of higher order cognitive tasks mature later during development but start declining in a relatively younger age [71, 72] Further, the recent review of Damoiseaux [15] also emphasizes on disrupted 'rich-club' organization in the older adults. The 'rich-club' comprises the same regions that are involved typically in higher-order cognitive tasks.

Excitingly, whole brain computational modeling of the resting state connectivity in the healthy adults [73] and animal models [74] reveal that the rich-club regions of the brain remain in metastable regime at rest and these same regions govern the dynamics of the whole-brain [21]. The PASA, HAROLD or CRUNCH theories are all based on the shifts of activity related to the prefrontal regions that are an important part of the rich-club. Hence, the over-activation observed in prefrontal and other rich-club regions during the task-condition might actually be due to the change in metastable dynamics of these regions during rest. In a unique study that compared effects of aging on FC during task and at rest, Geerligs and colleagues showed that age-related differences are not consistent across resting state and task conditions [75]. This finding points towards a need for better characterization of FC dynamics that can explain age-related changes across mental states. Arguments of compensation theories are based on the task-fMRI studies while support for the dedifferentiation hypothesis relies on the resting state data. The dynamical concept of metastability allows for the coexistence of compensation and dedifferentiation. According to this framework changes observed during task and rest are governed by the underlying metastable dynamics of the system and dynamic FC being more sensitive to the capturing the temporal changes, will be more suitable for understanding the age-related effects. Another prominent theory that argues for investigation of the lifespan dynamics is the 'scaffolding theory of ageing cognition' (STAC) [76], which proposed a scaffold network that might be developed during the maturation process but would no longer be used in adulthood as more optimized and efficient networks take over. Later in life, when the finely-honed networks start deteriorating, less efficient network scaffolds are recruited for maintaining the behavioural integrity. We suggest that this can be achieved by the self-organization of functional networks with age. Metastability allows flexibility of communication that might be reflected in the local

dynamics of the neural population, which in turn changes the long-range functional connectivity among regions. Subsequently, the use of alternate communication routes is operational in the face of declining structure. Evidences suggest that BOLD signal variability plays an important role in the outcome of aging-related changes as well as cognitive performance of the healthy adults [77]. Measures of metastability (e.g., Kuramoto Order Parameter) formally capture the variability in the synchronization patterns at network level from the BOLD data or from the neural data simulated by the whole-brain computational models. Thus, these measures can be used along with the longitudinal data to test the claims of STAC theory in analytically tractable manner.

In summary, dedifferentiation seems to be a rule, where brain networks reorganize themselves. Although age-related changes in connectivity are evident from many studies now, dynamics governing this reorganization is still an uncharted territory. Answer to this question would not only benefit investigations of aging but also in studies that target characterization of brain network reorganization at multiple scales. We propose that metastability is one such conceptual bridge that provides an integrative framework to understand the vast degree of structural and functional degeneracy in the brain network organization [78, 79]

2.2 Age-effects on Structural and Functional Networks

Age related network level changes in structural connectivity have revealed linear reduction of white-matter fiber counts across the lifespan [2]. Apart from average fiber counts, the structural changes were observed in the subtle decreases in fiber lengths of connections between hub-to-hub (highly central nodes of the network) and hub to non-hub (feeder) connections [3]. At least two cortical network-based studies have reported decreased modularity in the elderly population i.e. structural networks of elderly adults become less segregated than that of younger adults[80, 81]. For structural networks, the global and local measures of efficiency show characteristic inverted U-shaped curve with peak age in the third decade of life-span i.e. efficiency of these networks peak around the middle-age [82].Apart from these, there are no recent studies that discuss the age-related changes in structural networks.

When the functional networks are decomposed into modules such that inter-module connectivity is maximized and intra-module connectivity is minimized, they represent the known-resting state networks (RSNs). Similar to structural networks, functional networks also report age-related decrease in modularity i.e. distinct modules that are functionally independent in young adults tend to merge into a single module in the elderly adults. Global efficiency of functional networks is preserved with age while local efficiency and rich club index show inverted U-shaped curve with peak ages at around 30 years and 40 years, respectively. Patterns of functional efficiency across the cortex are not the same. Networks associated with primary functions such as the

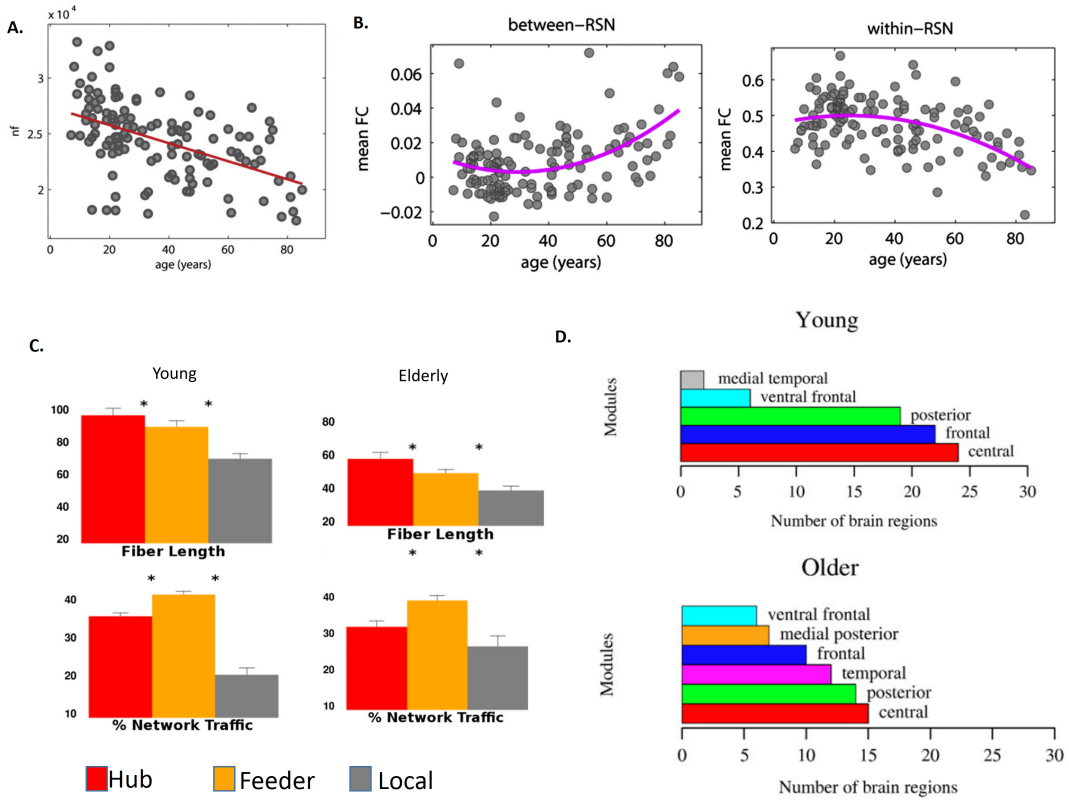

Figure 2.1: Structural(A,C) and Functional (B,D) Connectivity Changes Across Age. (A) Long-range white-matter fiber counts reduce across the lifespan, together with subtle changes in the roles of hub (hub-to-hub), feeder (hub-to-non-hub), and local (non-hub-to-non-hub) connections as depicted in subfigure (C). (B) Functional connectivity changes within and between resting-state networks are non-linear across the lifespan and cannot be fully understood in terms of structural changes. (D) Brain function becomes less modular with age, and functional modules become less distinct as modularity decreases. Abbreviations: FC, functional connectivity; nf, number of fibers; RSN, resting state networks. Subfigures (A) and (B) are adapted from [2], Subfigure (C) is adapted from [3] & Subfigure (D) is adapted from [4]

somatosensory and the motor networks maintain efficiency in the elderly, while higher-level processing networks such as the default mode network (DMN, [24]), fronto-parietal control network (FPCN, [83]), and the cingulo-opercular network [84] often show decline in efficiency. Some of these changes are depicted in 2.1. As can be observed, structural and functional networks show differential properties with age. Any comprehensive aging theory requires an account of all these changes in a single framework. The most direct evidence for changes in SC-FC relationship due to aging comes from Zimmermann *et al* [5] who used partial least square (PLS) regression to predict subject age based on the raw mean SC, FC values and SC-FC correlation among each network nodes. One interesting finding from this study is that there existed a pattern of SC-FC coupling which uniquely predicted age with high accuracy (r=0.73). Figure 2.2 shows these patterns. As can be observed in the figure, regions where SC-FC coupling

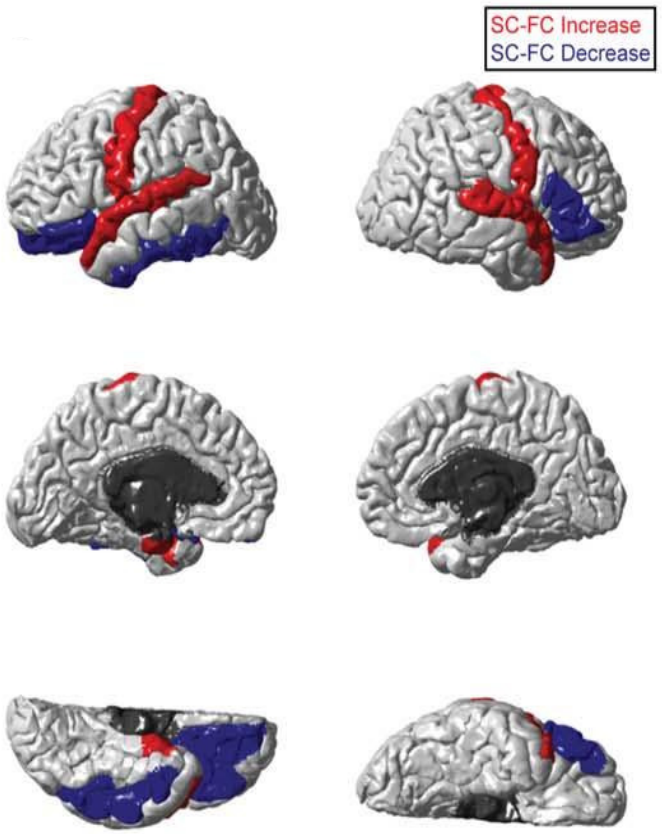

Figure 2.2: Brain regions where SC-FC coupling predicts age better than the SC or FC alone. Nodes in red depict increase in SC-FC coupling with age while nodes in blue represents decrease of coupling with age. Figure adapted from [5]

.

increased with age included L and R precentral and the L and R superior temporal gyrus which are part of sensorimotor network. While the SC-FC coupling weakened with age in L inferior temporal and the L and R pars orbitalis. The authors suggested that SC-FC coupling rather than SC or FC alone might be used as a bio-marker for predicting healthy aging.

All the above mentioned studies considered static approaches in the analysis of FC networks, and hence did not consider how the dynamics might play role in exploring SC-FC relationships. As discussed in previous chapter, metastability based hypothesis of aging requires to investigate temporal dynamics of signals. A few empirical studies independently explored dynamics of the BOLD signals and at least one study has explored the dynamics of the functional connectivity in the context of aging. We will review these studies in the next section.

2.3 Quantifying Age-related Changes in Brain Dynamics

Earlier empirical studies have used variance-based [85, 86] or multi-scale entropy [87] measures to characterize the moment-to-moment variability in EEG or BOLD signals. Although, these studies provided interesting insights into the complexity of the aging brain, they mostly investigated the variability of each region independently rather than looking at the 'network-level interactions' among these regions. The dynamic nature of FC is often not acknowledged by the current theories of aging. Indeed, FC can temporarily dwell around one stable network pattern and spontaneously fluctuate away towards another – a behaviour known as 'functional connectivity dynamics' (FCD) (See [88] for a review). While the origin of FCD is still an active area of research, FCD patterns have been shown to change during adulthood [89, 90] and during disease [23]. We argue that age-related dynamic changes need to be quantified in terms of FCD rather than the static FC in order to understand the dynamics of the aging brain better.

In a very recent study[91], Battaglia *et al.* analyzed time-varying functional connectivity and found that the speed of FCD (i.e. number of different FC configurations explored in time) decreases with age. Furthermore FCD properties predicted differences in cognitive performance between same-age subjects thus giving the first direct support to our hypothesis. In chapter 5, we will compare our results with the results from this study. In another such attempt, Schlesinger and colleagues recently investigated dynamic community structure and the flexibility of each node to switch between the communities while the subjects performed a memory task [92]. This study conclusively suggests that older subjects are more likely to switch between network configurations (more-stable networks) during task condition than are younger counterparts when both the groups performed equally well on the task. Similar conclusions were drawn from another methodologically distinct study [89] concluding that older adults explore more-fragmented network states. While both these theories suggest that older adults might achieve the task performance by flexible network reorganization. However, due to unavailability of the behavioral data for our dataset, we will not make any claims regarding the relationship between metastability and task-performance of elderly adults.

Chapter 3

Data Acquisition and Preprocessing

In this chapter, we describe in detail the dataset used for the studies [7][1]. We also explain the acquisition parameters and preprocessing steps required for the generation of the structural and functional connectivity networks.

3.1 Data

The MRI data was collected from 48 healthy participants (age 18-80yrs; mean: 41.55 years; 19 males) at the Berlin Centre for Advanced Imaging, Charité University, Berlin, Germany. All participants gave written informed consent and the study was performed under the compliance of laws and guidelines approved by the ethics committee of Charité University, Berlin. The distribution of ages is shown in Fig. 3.1. Since the participants were not uniformly distributed across all ages (and also due to cross-sectional nature of the study) we refrained from any regression analysis. Instead we further split them into three uniform age-groups: young (N=15, age: 18-27; mean: 23.25 years), middle-aged adults (N=17, age: 28-51; mean: 38.11 years) and Old (N=16, age: 54-80; mean: 65.2 years). All the further group-analyses were carried out on these cohort. The participants did not show any self-reported sign of age-related neurological or psychological conditions at the time of imaging. Mini Mental State Examination (MMSE) scores or any other behavioural scores were not available for analysis and hence we do not attempt to make any comments regarding the cognitive performance of these adults at the individual level. All our analyses and conclusions are strictly based on the chronological age of the participants.

[1]Prof. Dipanjan Roy would like to acknowledge the department of Neurology, Charité, Charitéplatz, Berlin for making the data available for this study and for his affiliation with the institute as postdoctoral research associate at the time of data acquisition.

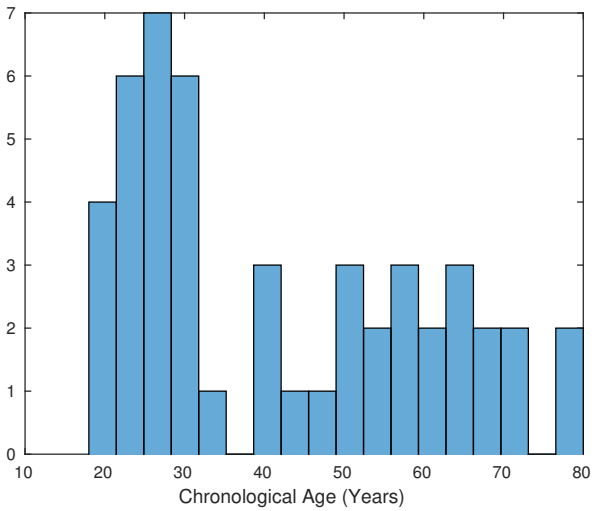

Figure 3.1: Distribution of participants' age.

Image acquisition Parameters

The scans were obtained using 3 Tesla Siemens Tim Trio MR scanner in two sessions. First the anatomical (T1 and T2) and diffusion weighted images were acquired and in the second session simultaneous EEG-fMRI recording was obtained for each participant. For fMRI session, the subjects were asked to remain awake but keep the eyes closed during the entire scanning session. No other controlled task was performed. The EEG recordings were acquired for the validation purposes of pre-processing pipeline but have not been used for the current analyses. However, specific measures were taken to address any artefact that might have been introduced due to the EEG electrodes. In the following sub-sections we discuss the acquisition parameters briefly before moving onto the pre-processing pipeline.

- **Anatomical(T1) MRI**
  For each participant anatomical T1-weighted scans (MPRAGE, TR:1900 ms, TE: 2.25 ms, 192 sagittal slices, voxel size: $1 \times 1 \times 1$ mm,FoV: 256 mm) as well as T2-weighted scans (2d turbo spin-echo sequence, TR: 2640 ms, TE1: 11 ms, TE2: 89 ms, 48 slices, voxel size: $0.9 \times 0.9 \times 3$ mm, FoV: 220 mm) were obtained.

- **Diffusion Weighted Imaging**
  Each participants were scanned for Diffusion-Tensor-Imaging (twice-refocused spin echo diffusion preparation; 64 different diffusion directions, b-value 1000 s/mm 2 , one b0 image recorded, TR 7500 ms, TE 86 ms, 61 transversal slices, voxel size $2.3 \times 2.3 \times 2.3$ mm, FoV 220 mm).

- **Functional MRI**
  Resting state functional MRI (BOLD-sensitive gradient echo 2d EPI, T2*-weighted, TR

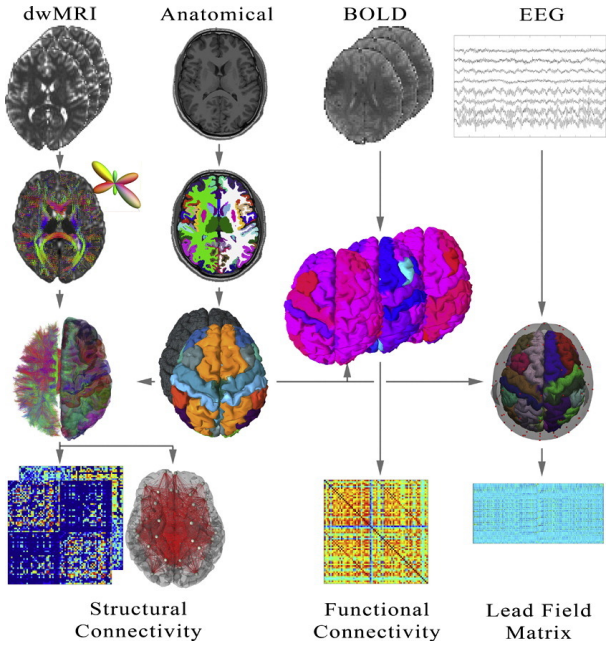

Figure 3.2: The Virtual Brain Preprocessing Pipeline. Each participant's diffusion tensor and functional images were registered to pre-processed T1-anatomical images. Subject-specific structural connectivity (SC) matrix was obtained by running probabilistic tractography for regions from FREESURFER's Desikan-Killiany atlas [6]. Functional connectivity (FC) matrix was obtained by computing Pearson correlation between regional mean time-series obtained from the preprocessed rs-fMRI images. EEG data has not been used for the current analyses and hence not relevant for the discussion.Figure adapted from [7]

1940 ms, TE 30 ms, 32 transversal slices, voxel size 3×3×3 mm, FoV 192 mm, 666 volumes) was recorded for approximately 22 minutes simultaneously to the EEG recording. First five volumes were dropped in the preprocessing steps for excluding possible saturation effects and hence total of T= 661 volumes were used for all further analyses in this thesis.

3.2 Preprocessing Pipeline and Connectivity Matrices

The Virtual Brain (TVB) pipeline was used for the preprocessing of the data and is graphically represented in Fig. 3.2. We briefly discuss the preprocessing steps used to arrive at the connectivity matrices. Detailed discussion on the validity of each of the steps involved in the pipeline is out of the scope of this thesis but is rigorously discussed in [7].

- **Anatomical MRI and Parcellation**
  In TVB, anatomical images are processed using Freesurfer's $recon-all$ command [2] and typical processing steps include motion correction, intensity normalization, skull strip-

[2] `https://surfer.nmr.mgh.harvard.edu/fswiki/recon-all`

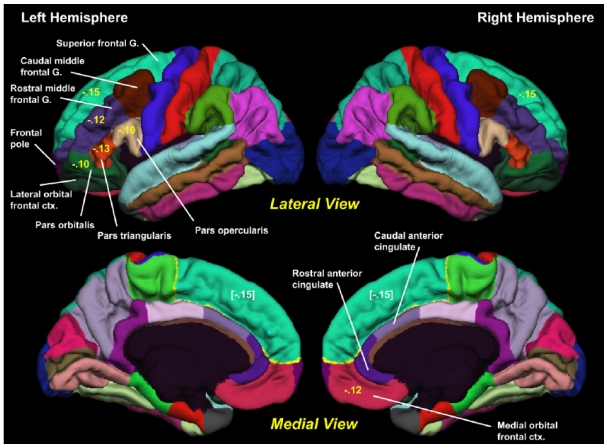

Figure 3.3: Desikan-Killiany Parcellation scheme used for defining nodes

ping, removal of non-brain tissue, brain mask generation, cortical reconstruction, WM and subcortical segmentation, cortical tessellation generating GM−WM and GM-pia interface surface-triangulations and probabilistic atlas based cortical parcellation. Desikan-Killiany atlas was used for parcellating the T1 images into $N = 68$ bilateral cortical regions throughout this study (Freesurfer IDs: 1001-1035 for left hemisphere and IDs: 2001-2035 for right hemisphere; IDs 1004 and 2004 correspond to bilateral corpus callosum and was removed from the analysis). The Freesurfer IDs for each cortical regions can be found online [3]. This parcellation is shown in figure 3.3. The 68 region names are enlisted in Table 3.1.

- **DW-MRI and Structural Connectivity Matrix**

  Pre-processing steps for diffusion MRI images typically involve motion correction, eddy current correction and registration with the subject-specific T1 image. This was performed in TVB using Freesurfer command *dt_recon*. Tractography requires binary white matter (WM) masks to restrict tracking to WM voxels. This segmentation is obtained by transforming the binarized WM segmented image from subject-specific anatomical space to diffusion space. Before we can run a tractography algorithm, diffusion tensor images (DTI) are to be constructed which store the ellipsoid of diffusion at each voxel. The strength of diffusion at each voxel can then be estimated using the fractional anisotropy (FA) calcualted from bval (Eigen values). The major axis (direction) of diffusion at each voxel location is also estimated using the eigen-vectors (bvec).These eigen vector maps were masked by WM segments. These steps were performed using MRTrix preprocessing. FA mask containing high anisotropy voxels is computed for subsequent fiber response function estimation. Finally the tractography algorithm was run by selecting nearest WM voxel from a particular GM parcellation (as previously defined) as seed or target mask. Tracks are terminated when they leave white-matter segment or reach to a target mask

[3] `https://surfer.nmr.mgh.harvard.edu/fswiki/FsTutorial/AnatomicalROI/FreeSurferColorLUT`

Table 3.1: Labels for Desikan-Killiany Atlas. The first and second ID in ROIs represent left and right hemisphere regions respectively.

ROI #	Region Name
1,35	bankssts
2,36	caudalanteriorcingulate
3,37	caudalmiddlefrontal
4,38	cuneus
5,39	entorhinal
6,40	fusiform
7,41	inferiorparietal
8,42	inferiortemporal
9,43	isthmuscingulate
10,44	lateraloccipital
11,45	lateralorbitofrontal
12,46	lingual
13,47	medialorbitofrontal
14,48	middletemporal
15,49	parahippocampal
16,50	paracentral
17,51	parsopercularis
18,52	parsorbitalis
19,53	parstriangularis
20,54	pericalcarine
21,55	postcentral
22,56	posteriorcingulate
23,57	precentral
24,58	precuneus
25,59	rostralanteriorcingulate
26,60	rostralmiddlefrontal
27,61	superiorfrontal
28,62	superiorparietal
29,63	superiortemporal
30,64	supramarginal
31,65	frontalpole
32,66	temporalpole
33,67	transversetemporal
34,68	insula

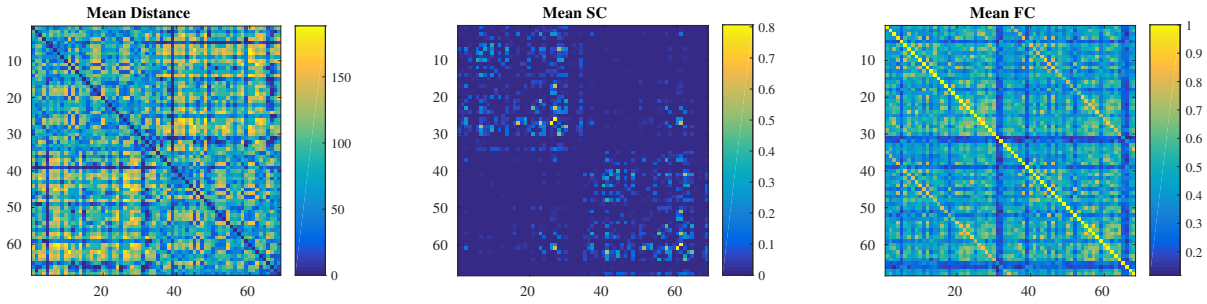

Figure 3.4: Mean distance (left), structural (center) and functional connectivity (right) matrices averaged across all subjects

seed. Considering one region as seed and all others as target mask at a time, the tractography is performed. In order to resolve crossing pathways, fibers are prolonged by employing a probabilistic tracking approach as provided by MRTrix. Probabilistic tractography in MRTrix is based on a constrained spherical deconvolution (CSD) that computes the fiber orientation distribution function (fODF) for each image voxel (see MRTrix documentation [4] for more details). To address several confounds in the estimation of connection strengths (information transmission capacities), a new seeding and fiber aggregation strategy was employed for this pipeline and is described in detail in [7]. After the fiber tracking, several connectivity measures were used for defining connectivity matrices. For the studies here we have mainly used two of these matrices: 1. Average aggregated distance matrix ($SC\_dist\_mean\_agg$) that measures average length estimated by all the tracks between a pair of regions (referred as distance matrix henceforth). Mean distance matrix averaged across all subjects is shown in Fig 3.4 (left). 2. Region-wise Capacity Matrix ($SC\_file\_bwflav1\_norm$) that estimates average normalized connection strengths from all the distinct connections found on single-voxel level between pairs of regions i.e. Structural connectivity matrix i.e. the structural connectivity matrix. Fig 3.4(Center) shows the SC matrix obtained by this method averaged across all subjects.

- **rs-fMRI and functional connectivity matrix**
  Preprocessing steps for resting state data was performed using FSL's FEAT pipeline [5] and steps included deleting the first five images, high-pass temporal filtering (100 second high-pass filter), motion correction, brain extraction and a 6 DOF linear registration to the MNI space. Then, BOLD volumes are registered to the subject's T1-weighted images and parcellated according to FREESURFER's cortical segmentation. By inverting the transformation rule found by registration, anatomical segmentations are mapped to the functional space and average BOLD signal time series for each region are generated by computing the spatial mean for all voxel time-series of each region. From the region-wise aggregated BOLD data, functional connectivity (FC) matrices are computed within

[4] http://mrtrix.readthedocs.io/en/latest/
[5] `https://fsl.fmrib.ox.ac.uk/fsl/fslwiki/FEAT/UserGuide`

MATLAB using pairwise Pearsons's linear correlation coefficient. Fig 3.4 (right) shows this FC matrix averaged across all subjects.

Chapter 4

Network Analysis

4.1 Introduction

Brain networks – both structural and functional, have the properties of the complex brain networks. These include, power-law degree distribution, existence of central nodes known as hubs, modular architecture, higher participation coefficient and lower average shortest path length than that of the random networks. These properties suggest the balance between information segregation and integration which is the property of a metastable systems. As seen in the previous chapter, age can affect some of these network measures and in turn disrupt the balance between integration and segregation. These age-related structural disruption and functional reorganization can be systematically studied using graph-theoretic complex measures. Apart from the studies mentioned in Chapter 2, no study till date has explored comprehensive list of complex network measures. Hence, to validate our dataset and to compare the three age-groups in terms of their SC and FC network measures, we study integration and segregation measures for our dataset.

4.2 Methods

We used the structural and functional connectivity (SC and FC) matrices obtained from the Berlin dataset (explained in the previous chapter) to study the age effect on six network measures: Global Efficiency, Average Local Efficiency, Clustering Coefficient, Characteristic Path Length, Small-worldness and Modularity. The global efficiency and charateristic path length gives the measure of integration of the network while clustering coefficient, local efficiency and modularity are the measures of segregation. Small-worldness can be related to the overall complexity of the brain-networks. The average SC-FC matrices as obtained from the post-processing of DTI and fMRI data are shown in Figure 3.4. Subject specific SC-FC matrices were first nor-

malized and scaled to have values between 0 to 1. Enforcing this scaling allowed to remove the negative weights from the FC matrix. Although most graph theoretic algorithms have an implementation for the negative edge-weights, most of these treat the negative weights as the least preferred path while in correlational networks, higher negative weights might have important network features. However, generalizing the complex network measures for signed correlational networks is still an important area of research in the domain of complex networks [93]. Hence due to lack of interpretability of the results in case of negative weights, we circumvent this issue by min-max scaling of FC matrix. All the network measures were calculated using the Brain Connectivity Toolbox (BCT) [94]. Each network measure was then separately compared among 3 age groups: Young (18-27yrs), Middle age (28-51 yrs) and Old (54-80 yrs). We explain in detail the methods for network generation, network measures and statistical analysis of these measures in the next subsections.

4.2.1 Thresholding and Network Generation

Statistical network analysis often introduce false-positive (FP) associations. In SC, FP edge-weights arise due to streamline estimation during the tractography algorithms and for FC, the FP rate is high due to estimating large number of correlation coefficients. To avoid influence of FP on group-comparisons, here we applied proportional thresholding under the assumption that weaker edge-weights in both SC and FC networks arise due to high false-positive rates. For each subject, each of the network was sparsified over range of thresholds between 1%-50% (threshold t=$0.01 \cdots 0.5$) proportion of all the weights for both SC and FC matrices. Moreover, the diagonal entries for both matrices were forced to be zero for avoiding self-loops.

4.2.2 Network Measures

For each subject, six global network measures were calculated for both FC and SC, at each threshold: Global Efficiency, Clustering Coefficient, Characteristic Path Length, Small-worldness and Modularity. Each of these measures were defined as follows:

- Characteristic Path Length (CPL): Mean of shortest paths between each pairs of nodes in the network. That is, average steps required along the shortest path to reach from any node of the graph to any other node. For weighted undirected network, it is defined as follows:

$$CPL^w = \frac{1}{n} \sum_{i \in N} \frac{\sum_{j \in N, j \neq i} d_{ij}^w}{n-1}$$

  where N=68 (i.e. total number of nodes) and d_{ij}^w defines the weighted distance of the shortest path between a node-pair (i, j).

- Global Efficiency (EGlob): The inverse of the harmonic mean of shortest path length between each pair of nodes within the network. For weighted undirected networks, it is defined as follows:

$$Eglob^w = \frac{1}{n}\sum_{i\in N}\frac{\sum_{j\in N, j\neq i}\left(d_{ij}^w\right)^{-1}}{n-1}$$

  Note that the global efficiency is inversely related to the characteristic path length. However, it is numerically easier to compute than characteristic path length when the graph becomes sparse. Moreover, it also captures group differences better than the CPL for sparser graphs.

- Clustering Coefficient (CC): It is a local (nodal measure) and is defined as the mean fraction of neighboring nodes of a node which are also neighbors of each other. It is calculated as average geometric mean of all triangles associated with the node. Clustering coefficient was averaged across all nodes to obtain the mean CC of network. Mean clustering coefficient can be defined as follows for the weighted undirected graph:

$$CC^w = \frac{1}{n}\sum_{i\in N}\frac{2t_i^w}{k_i(k_i-1)}$$

  where, k_i is weighted degree of node i and t_i^w is geometric mean of weights of triangles around node i. If the nodes j and h are neighboring nodes of node i (and if $\exists$ edges between i and j, j and h and between i and h having weights w_{ij} , w_{jh} & w_{ih} respectively) then, t_i^w is defined as follows:

$$t_i^w = \frac{1}{2}\sum_{j,h\in N}\left(w_{ij}w_{ih}w_{jh}\right)^{\frac{1}{3}}$$

- Local Efficiency (Eloc): Average global efficiency of each node i of the sub-graph that contains neighbours of i. Eloc is the measure of the fault tolerance of the system. It is defined as

$$E_{loc}^w = \frac{1}{2}\sum_{i\in N}\frac{\sum_{j,h\in N, j\neq i}\left(w_{ij}w_{ih}\left[d_{jh}^w(N_i)\right]^{-1}\right)^{\frac{1}{3}}}{k_i(k_i-1)}$$

  Where the notations are same as previously defined.

- Small-World Index (Sw): Sw was calculated as the ratio of normalized mean CC and normalized CPL. Networks having higher clustering and lower characteristic path lengths have high communicability and hence have higher Sw. For weighted network it was measured as follows:

$$Sw = \frac{(CC^w)(CPL^{rnd})}{(CPL^w)(CC^{rnd})}$$

Where CC^{rnd} and CPL^{rnd} are respectively the clustering coefficient and characteristic path length of the randomized weighted network. For our purpose we generated 10 randomized networks preserving the degree distribution of the original network each time and by rewiring each edge in the original network approximately twice. For each randomly generated network, we find CC & CPL after each iteration. Finally, CC^{rnd} and CPL^{rnd} were calculated by averaging values of CC and CPL across these 10 iterations. This procedure was repeated for each subject and for all thresholds to obtain the final values of Sw.

- Modularity (Q): Modularity was estimated using the Louvain community detection algorithm (see next section). It is calculated as the fraction of edges that falls inside the same communities compared to such edges between communities.For a given community structure, it is defined as follows:

$$Q = \frac{1}{2m} \sum_{ij} [W_{ij} - \frac{k_i k_j}{2m}] \delta(c_i, c_j)$$

Where W_{ij} is the weight of edge between nodes i and j, k_i & k_j are weighted degree of nodes i and j respectively, m is the sum of all edge-weights in the graph, c_i & c_j are community assigned to nodes i and j respectively and δ defines the Kronecker delta function. Since modularity depends on a particular community structure and community detection itself is an optimization process, we need to approximate value of modularity across several runs of modularity optimization. This optimization algorithm is explained in details in the next section.

4.2.3 Community Detection

To construct the most representative structure of network of communities, in order to compute the modularity, we applied Louvain algorithm [95]. We chose a random partition containing 4 modules (the most common number of modules identified over 100 independent realizations of the algorithm) as our representative partition and the similarity of this chosen partition with 99 other modularity iterations of the group average matrix was calculated using normalized mutual information and this was used to get the final consensus partition using a threshold of at least 80 similar assignments of an area to an individual cluster over the N=10 runs of the algorithm. Modularity was calculated as the mean of all the modularity values obtained across these 10 runs.

4.2.4 Statistical Analysis

Pairwise group differences for each network measure were analyzed separately for SC and FC among three age-groups using non-parametric one-way ANOVA, i.e., Kruskal-Wallis rank test [96].

4.3 Results

We studied 5 global network properties across lifespan in order to understand the differential effects of aging on structural and functional connectivity and to validate our dataset in that process.

- **Characteristic Path Length (CPL)**
  Figure 4.1(A) depicts the effect of network sparsity on the *CPL* of the three groups-young (green), middle-aged(blue) and old (red). Since *CPL* is function of shortest path distances in the graph, the CPL exponentially decreased with the decrease in network sparsity (increase in the threshold for preservation of edges). This trend was clearer in case of SC than in FC. For SC, at very sparse networks ($t = 0.01 \cdots 0.03$), *CPL* of younger subjects were higher than that of the other two groups however, this did not result into any significant differences among the three group-means ($p >> 0.05$). Similarly for Functional Connectivity (FC), no significant changes across the three groups were observed.

- **Global Efficiency (Eglob)**
  Figure 4.1(B) shows the effect of network sparsity and age on the global efficiency of the network. Since global efficiency is inversely related to the shortest path distances of the networks, *Eglob* exponentially increased as the function of network sparsity, both for SC and FC. The *Eglob* of SC network consistently showed group differences between young to old age-groups and between middle-age and old groups at all sparsity levels (threshold $t > 0.04$). In particular, younger and middle-aged subjects showed significantly higher global efficiency ($p < 0.05$) as compared to that of the older subjects. However, there were no significant differences among any of the age-groups across any threshold in the FC network.

- **Clustering Coefficient (CC)**
  Figure 4.1(C) plots the clustering coefficient of networks at different sparsity levels for three different age-groups. As can be shown, there were no significant differences in the clustering coefficient for the SC networks. However, for denser FC networks ($0.4 < t < 0.5$), clustering coefficient of the younger subjects were higher than that of the middle-aged subjects. While no significant changes were observed for older subjects. With increased

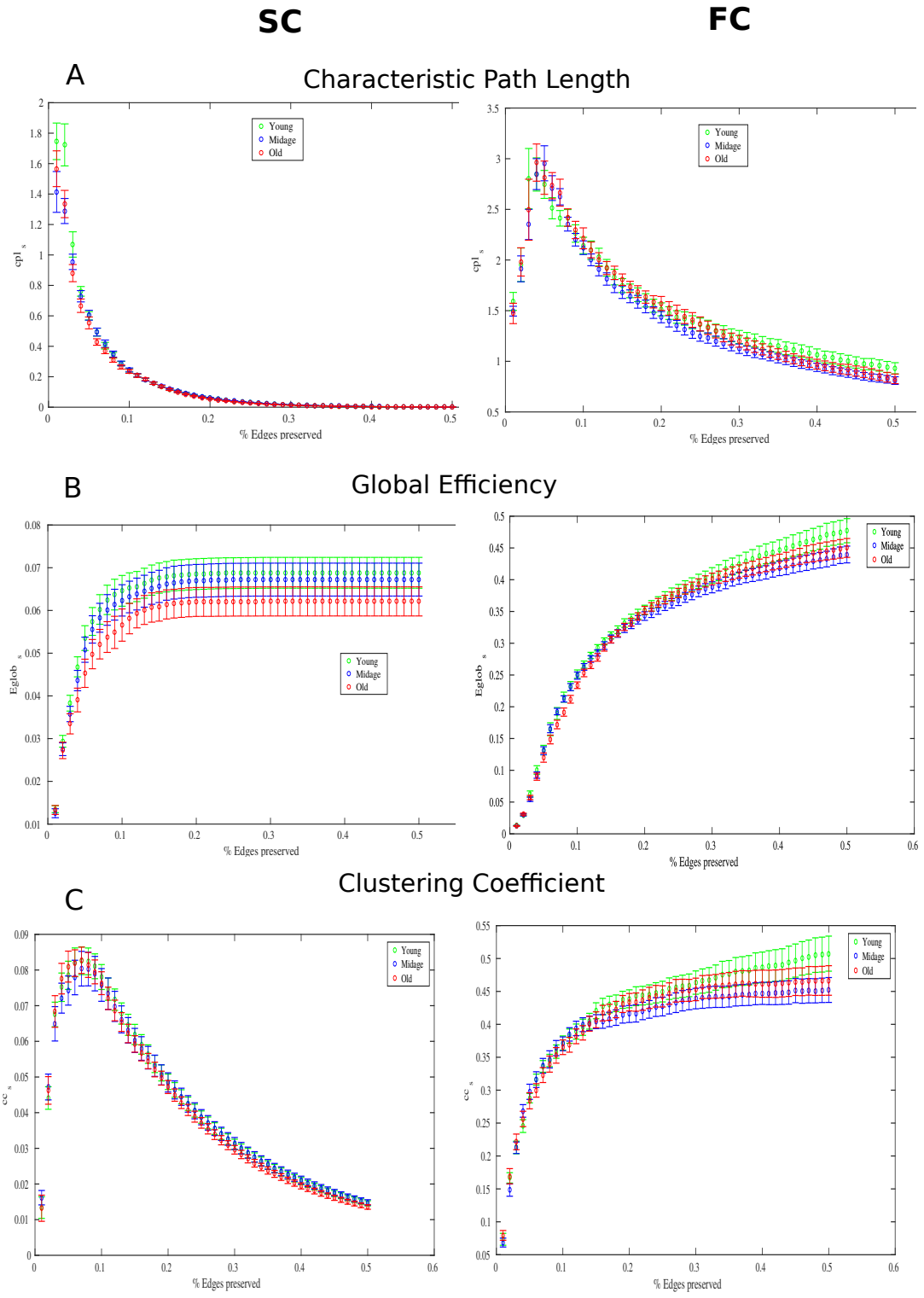

Figure 4.1: Group differences in SC(left panel) and FC(right panel) network measures: (A) Characteristic Path Length, (B) Global Efficiency and (C) Clustering Coefficient across different levels of network sparsity (X-axis). The error-bars represent standard error to the group means.

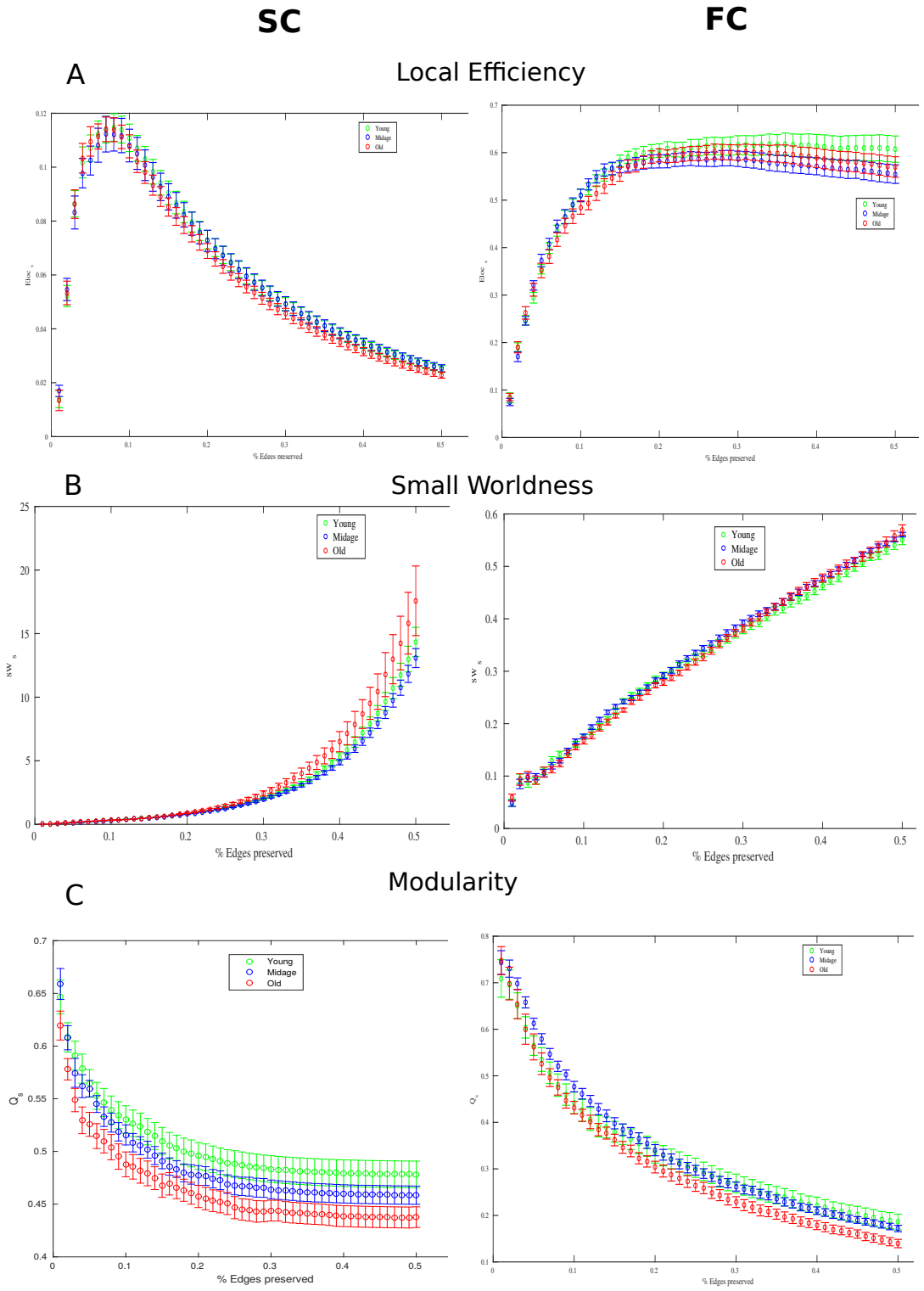

Figure 4.2: Group differences in SC(left panel) and FC(right panel) network measures: (A)Local Efficiency Path Length, (B)Small-worldness and (C)Modularity across different levels of network sparsity (X-axis). The error-bars represent standard error to the group means.

value of t, the number of edges (having weaker correlation values or edge weights) increased in the network. This suggests that for younger subjects, increase in the weaker correlations resulted into more segregated clusters in comparison with the middle-aged group.

- **Local Efficiency**
  Figure 4.2(A) plots the local efficiency of networks at different sparsity levels for three different age-groups. In SC matrix, local efficiency of the denser networks($0.4 < t < 0.5$) were significantly different across young and old as well as across middle-aged and old groups ($p < 0.05$). However, local efficiency of FC networks showed variable effects of age depending on the threshold of investigation. For example, at the smaller threshold (in sparser networks) *Eloc* of middle-aged group was higher than that of the older age-group. But in the denser network, *Eloc* of middle-aged age-group significantly reduced with compared to the other two age-groups.

- **Small-World Index**
  Figure 4.2(B) plots the small-world index across age-groups for all thresholds. No significant differences were observed either in the structural or functional brain networks for SW index, thereby suggesting no age-effect on this measure.

- **Modularity**
  Modularity determines how well a given graph can be decomposed into sub-graphs. It is a measure of segregation. As can be seen clearly from Figure 4.2(C), Modularity of SC networks was significantly different across all the three age-groups. Modularity of SC consistently decreased with age, suggesting that structural networks became less distinct with age. For the functional brain networks as well, modularity of the older groups showed significant decreases from that of the younger group. As the network grew denser, the modularity differences between older and middle-aged group also became prominent.

4.4 Discussion

We measured graph theoretical metrics for structural and functional brain connectivity across three age-groups: young, middle-aged and old at different network-sparsity levels. We discuss the results in this section.

- **Structural Connectivity Network**
  The network measures that showed the most significant differences across the three age-groups in SC networks were: Modularity, Local Efficiency and Global Efficiency. In particular, the modularity of the young adults was the highest, followed by that of the middle-aged, followed by the older adults. This suggests that the structural network becomes less

segregated with age. i.e. Communities become less separable from each other. Wu et al. had previously shown that the modularity of the networks obtained by simply correlating the gray matter volume of each distant brain regions is lower in other older adults than in the other two groups [80]. Our results complement this by suggesting that the white-matter structural network start deteriorating even earlier, around the middle-age. Global efficiency of the elderly showed significant decrease from the other two-groups. Previously, a study has found an inverted U-shaped curve for Global efficiency of SC networks [82] with peak age at around 30 years of age. We found the significant differences only among middle-aged to old group (and not between young to middle-aged). This is precise;y because this study included participants from the age-group 9-18 years and hence, their study includes age-effects related to adolescent development as well. Local efficiency of older adults was significantly lower than the other two groups, but not consistently across all thresholds. This result is in accordance with the results observed by [2] but should be taken with caution since it stands only for the selected few higher thresholds.

- **Functional Connectivity Network**
  Functional Connectivity showed significant age-effects in modularity, Local Efficiency and Clustering Coefficient, but not in Global Efficiency unlike SC. Since the FC showed differences only in the measure of information segregation, it confirms the results from the previous studies which show that the functional networks become less segregated or functionally less specialized with age. We found significant differences in clustering coefficient. Previous studies by Betzel *et al.* has shown that the between network RSN connectivity increases with age while within network connectivity reduces [2]. Our results support this result and also report the dedifferentiation as described in the previous chapter. Clustering coefficient only showed significant differences across young to middle aged and only for the higher thresholds. This is in accordance with the results from [82] that also showed using linear regression analysis, that the clustering coefficient of the functional networks showed slightly U-shaped trajectory, with the bottom value spanning in the fourth decade.

In summary, the age-related changes in SC and FC are not symmetric. While the global and local efficiency of structural networks decreased with age, FC networks only show significant age-effect in Local efficiency but not in global efficiency. Clustering coefficient declines with maturity (from young to middle age) but only in case of functional connectivity, not in structural connectivity. The only change common across both the modalities was the decreased modularity of the elderly adults in structural and functional connectivity networks. These results increased support for dedifferentiation hypothesis that suggests that the functional networks become less specialized with age. Here we did not investigate the nodal network properties since we are more interested in the global network phenomena. However, as discussed in the previous section, many studies have investigated this before and the comprehensive review of which can be found in [15].

Chapter 5

Predicting and Measuring Metastability in Aging Brain

5.1 Introduction

In previous chapters using whole-brain graph theoretical measures we demonstrated that age-related changes in functional and structural connectivity show different trends. Main observation from this analysis was that while global efficiency of structural networks significantly declines from young to old age-group, that of functional connectivity is maintained till the later age. Moreover, modularity of structural and functional networks showed differential patterns across thresholds. These network changes have been hypothesized to co-occur with the reduced task-specificity of functional networks during positive task performance [97], which might suggest flexibility of functional networks on top of declining structure [76, 64, 98].

However, in these studies we used static functional connectivity measures, the FC averaged over all time-points. However, recent evidences propose that functional organization of the brain at rest has rich dynamic repertoire, fluctuating between various possible states in time [20]. The change in dynamic-FC (d-FC) with age predicts brain maturity with good accuracy [90]. Flexibility of d-FC, known as 'metastability', also correlates with flexible cognitive function [99]. Since elderly adults show change of behavioral strategies [100] and also altered spatiotemporal FC patterns, we hypothesize that: 1) metastability of resting state FC will vary significantly across age-groups and 2) age-effect on metastability would manifest differently across different resting state networks. We adapt an exploratory analysis approach to verify these hypotheses. First, using signal processing techniques on BOLD time-series data, we improve temporal resolution of the imaging data and define metastability. Secondly, using graph theoretic approach, we detect communities that are consistent across age-groups. We investigate the significance of the first hypothesis of different metastability across age-groups in detected communities and in the whole brain. Furthermore, we divide brain regions into seven predefined functional networks namely: Control, Default Mode Network (DMN), Dorsal Attention Network (DAN), Ventral

Attention Network (VAN or salience network), Limbic System, Sensorimotor (SMN) and Visual Networks. We first assess age-effects on each of these individual networks. Finally, to test the second hypothesis of changed roles of resting state systems, we carry out discriminant function analysis (DFA) which explores linear combinations of these seven resting-state networks that contribute maximally in discriminating between healthy young, middle-aged and old subjects.

5.2 Methods

Figure 5.1 contains the work-flow for this analysis. Regional BOLD signal time-series data were obtained for 48 healthy participants from the Berlin data set described in Chapter 3. For the purpose of group level analysis in this study, subjects were further uniformly divided as follows: 16 healthy young adults (age: 18-27; mean: 23.25 years), 16 healthy middle-aged adults (age: 28-51; mean: 38.11 years) and 16 healthy old adults (age: 54-80; mean: 65.2 years). Imaging protocol and preprocessing steps are as explained in the chapter 3. Subject-specific functional connectivity (FC) matrices were obtained by applying z-transformed pairwise Pearson correlation between each pairs of regional BOLD time-series as well as using phase-synchrony between each pairs of filtered analytic BOLD signals (described in the next section).

5.2.1 Synchrony and Metastability

Each subject's regional BOLD time-series signals were first band-pass filtered in narrow frequency-band 0.04-0.07Hz using Parks-McClellan optimal equi-ripple filter [101]. Analytic signal (y_n) was derived from each band-pass filtered original BOLD signal as follows:

$$y_n(t) = x_n(t) + jH(x_n(t)) = Re^{i\phi_n(t)} \tag{5.1}$$

Where, $H(x_n(t))$ represents Hilbert transform of the original signal $x_n(t)$ for the n^{th} ROI. Analytic signal has advantage over original signal since it discards negative frequency components without loss of information and makes instantaneous phase ($\phi(t)$) of the signal accessible; hence allowing to explore relationships at higher temporal resolution. For each subject, at each time-point, the Kuramoto Order Parameter (R) then defines mean phase synchronization or instantaneous coherence in the network [59]:

$$R_c(t) = \frac{1}{N_c}|\sum_{j=1}^{N_c} e^{i\phi_j(t)}| \tag{5.2}$$

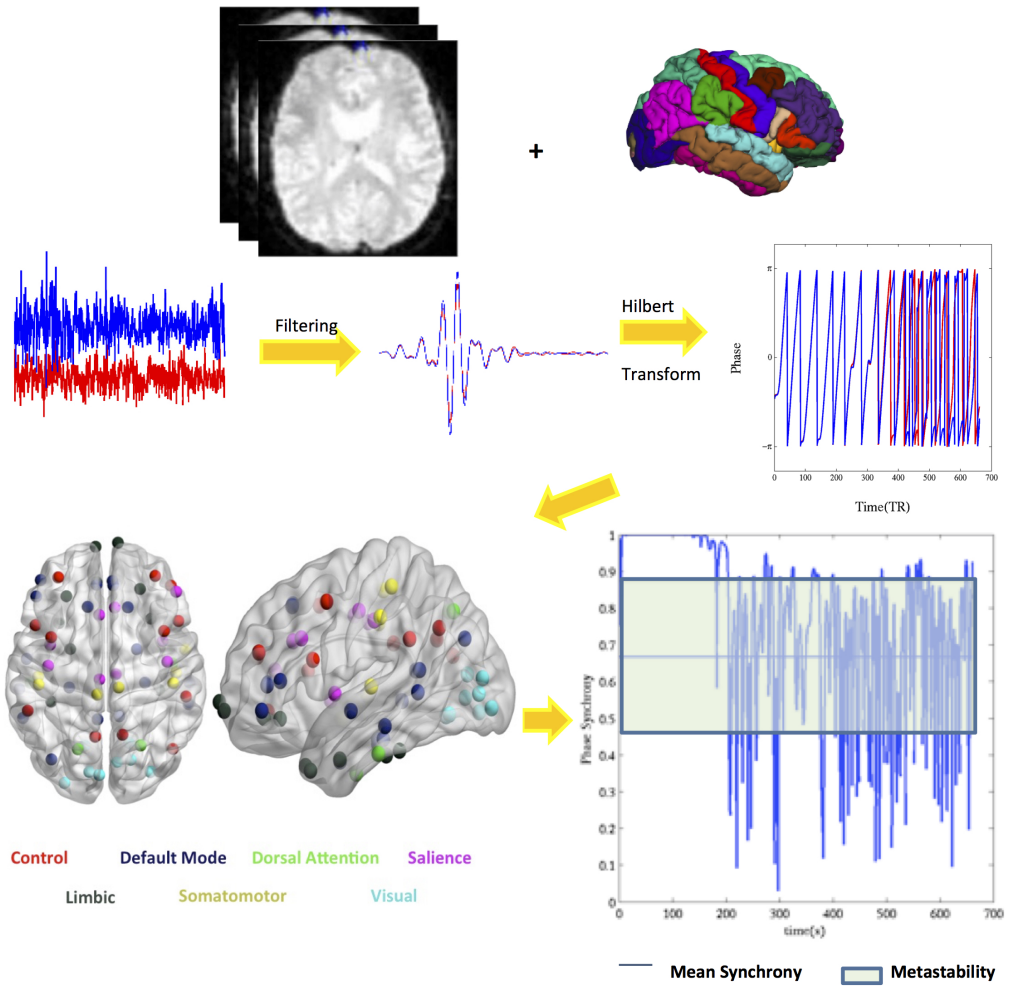

Figure 5.1: Illustration of the pipeline followed to characterize metastability. Preprocessed data is parcellated and regional BOLD signal is extracted. Hilbert transform is applied to filtered BOLD signals to find phase synchrony and metastability. Centers of the regions categorized in seven resting state networks identified in Yeo et al [8] and adapted for the Desikan-Killiany atlas used for this study.

Here, N_c represents the number of regions in the network c. For whole-brain analysis, $N_c = 68$; for the functional network analysis, N_c depends on the number of regions considered for that particular functional network. Metastability (ξ) for each subject is then defined as the amount of variability of brain-wide or community-wide coherence i.e., standard deviation of the Kuramoto Order Parameter.

$$\xi_c = \frac{1}{t-1}\sum_{t=1}^{T}(R_c(t) - \langle R_c(t)\rangle)^2 \tag{5.3}$$

We use this measure of metastability to compare across age groups as well as across lifespan.

Furthermore, subject specific functional connectivity matrices were obtained based on the instantaneous phase of the signal such that each entry FC_{ij} in the phase-based matrix FC represents cosine of instantaneous phase-difference between regions i and j $(\phi_i(t) - \phi_j(t))$ averaged over time [21]. These matrices were used for community detection (explained in next session) across subjects.

5.2.2 Community Detection & Hub Identification

Brain Connectivity Toolbox [94] was used to investigate the modular organization of each participant's FC networks. Modularity quality (Q) was determined by comparing the observed within-module connection density to the expected within-module connection density as explained in the previous chapter. Optimal community structure was obtained by maximizing Q-value for each partition according to the Newman's algorithm [102]. The modularity algorithm was run for 1000 iterations for each participant's FC. An optimal representative partition was determined with an iterative consensus-clustering algorithm, based on similarities in the 1000 near-optimal community partitions. Depending on the partition, hub regions were determined as the regions whose participation coefficient was greater than mean plus first standard deviation of all participation coefficient values for the subject's community partition. Most consistent hubs across all subjects were than used as seeds to determine the communities, which were common across all subjects. Same procedure was repeated for the FCs obtained based on Pearson Correlation and phase-synchrony. As shown in Fig. 5.2, number of communities detected was similar regardless of the method used for obtaining FC matrix. However, the phase-based FC determined fairly consistent communities across subjects. Apart from the communities obtained from the above procedure, we also subdivided each region of the brain in seven overlapping functionally important networks previously identified by Yeo et al [8]. Taking overlapping networks into consideration allow us to perform exploratory analysis to determine role of each of these networks in classification of healthy young, mid-age and old subjects.

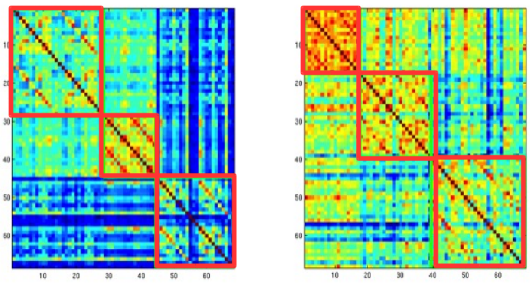

Figure 5.2: Communities detected (red bordered blocks) by correlation-FC (left) and phase-based FC (right) average connectivity matrices. The detected communities are the same for both the measures. Quality (modularity) of modular decomposition of phase-based FC matrix is lower for mean FC but no significant differences were found between the two modularity scores across subjects.

5.2.3 Statistical Analysis

For group-level analysis, non-parametric one-way analysis of variance was performed using Kruskal-Wallis rank-test [96]. Post-hoc multiple comparison tests were performed if required to understand pairwise group-differences [103]. To understand combined contribution of metastability scores of each of the seven resting state networks, we adapted Linear Discriminant Analysis [104] considering seven resting state networks scores as features and assigned age-group as class-labels.

5.3 Results

5.3.1 Metastability of elderly adults is significantly higher than that of middle-aged adults

Kruskal-Wallis rank test was used for comparing median ranks across young, middle-aged and old group. The one-way ANOVA test confirmed that there was statistically significant difference between metastability of young, middle-aged and elderly groups ($H(2) = 6.55, p = 0.038$) with a mean rank of 25.31 for young, 18.68 for mid-age and 31.41 for old group. A *post-hoc* ScheffeâĂŹs test showed that metastability of elderly adults differed significantly from that of the middle-aged subjects at p=0.038. No significant differences were observed between mean ranks of the other two pairs of groups. Fig. 5.3 summarizes the group-wise statistics in box-plot. These results confirm that metastability of elderly adults is significantly higher than that of middle-aged adults.

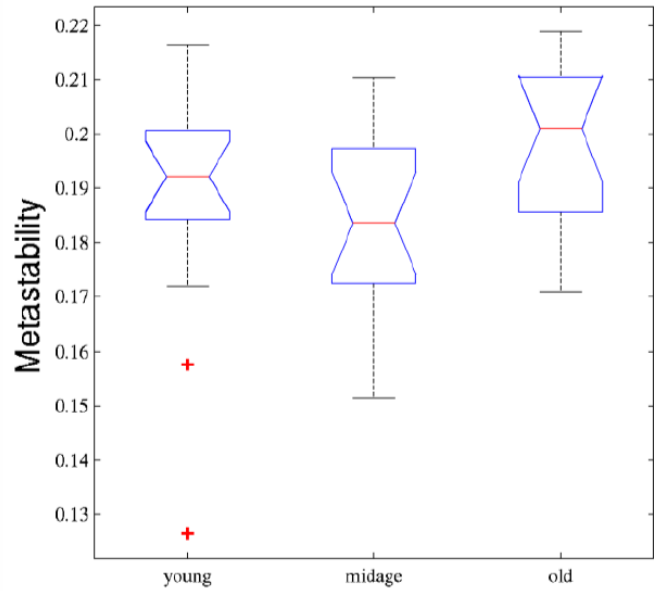

Figure 5.3: Box-plot for whole-brain metastability at rest for three age-groups. Horizontal lines represent mean ranks, notches represent 95% confidence interval. Mean rank of middle-aged group is significantly less than that of old group ($p = 0.038$).

Similar analysis was performed for the three communities obtained as discussed in above section. Mean values of metastability followed a U-shaped trend across age groups, with middle-aged subjects demonstrating the lowest metastability in all the communities. However, not all of these results were significant. Fig. 5.4 shows mean measures of metastability (standard error) across all communities. Metastability of elderly adults in control/attention network ($H(2) = 10.67$, $p = 0.0048$) was significantly different than that of middle-aged subjects. No significant age-effects were observed in the metastability of other communities.

5.3.2 Metastability of known functional network shows statistically significant differences across age-groups

As shown in previous analysis, metastability of middle-aged and old age groups across detected communities was significantly different. To gain understanding of functional importance of metastable regions involved in these communities, we further assigned each region to one or more resting state functional networks following the procedure from [105]. Metastability of each functional network for each subject was calculated as the standard deviation of temporal coherence of regions involved in these networks as explained previously. First, non-parametric univariate Kruskal-Wallis tests were performed for test of equality of group means on each of these networks. Results are summarized in tables 5.1 and 5.2.

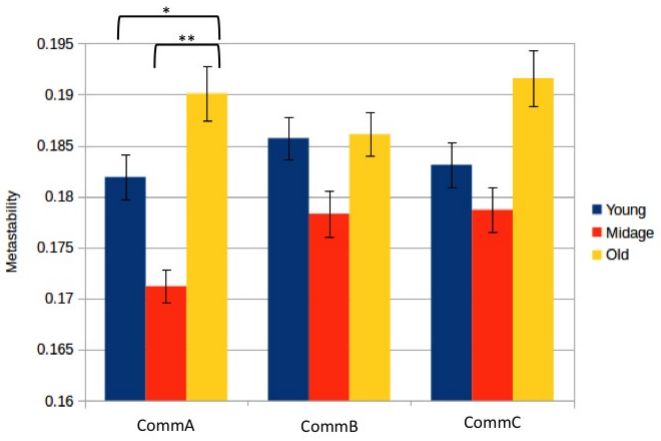

Figure 5.4: Metastability of the most consistent communities across subjects as shown in Fig 5.2. CommA: control and ventral attention regions (identified hub: Insula) CommB: Default Mode & limbic regions (identified hub: Precuneus); CommC: Sensorimotor regions (identified hub: Precentral gyus), $^{**}p < 0.005$, $^{*}p < 0.05$, Kruskal-Wallis test of mean ranks).

Table 5.1: Univariate test for equality of means

	Chi-sq	**sig**	**young**	**mid-age**	**old**
Control	6.43	.040*	30.94	18.44	26.03
DMN	3.74	0.154	21.94	22.56	30.66
DAN	10.72	.004*	25.81	16.74	32.97
VAN	11.85	.003*	29.5	15.38	30.72
Limbic	7.94	.018*	21.75	20.32	33.22
SMN	4.35	0.114	24.88	20.03	30.41
Visual	4.53	0.104	19.88	24.56	30.59

Table 5.2: Post-hoc Multiple Comparisons

	Post-hoc	**p-val**
Control	Young-midage	0.032
DMN	NA	-
DAN	midage-old	0.032
VAN	young-midage	0.0127
	midage-old	0.0058
Limbic	midage-old	0.0259
SMN	NA	-
Visual	NA	-

5.3.3 Linear Discriminant Analysis (LDA) and Importance of RSNs

Since metastability of different networks seem to be affected differently with age, we perform LDA to investigate which linear combination of the resting state network metastability values can help discriminate between the three age-groups significantly. The metastability measures of 7 RSNs (predictors) were transformed into two-dimensional orthogonal space (defined by basis DF1 and DF2, referred as functions hereafter), which maximally discriminate between the age groups. Chi-square test of Wilk's lambda confirmed that the predicted model parameters are statistically significant (See table 5.3). Loadings of each observed variable on the two functions is plotted in Fig 5.5. DF1 reflects the well known organization [31, 83] of 'task-positive' (namely Control, Dorsal and Ventral attention systems) and 'task negative' Default mode network. DF2 revealed interesting pattern of co-ordination between DMN and Control networks, which contrasts with attention networks. Sensorimotor, visual and limbic systems negatively contribute to DF1 but positively contribute to DF2.

All groups were successfully discriminated on the two axis (Fig. 5.6. 72.9% of original grouped cases were correctly classified by the discriminant function. Leave-one out cross-validation resulted in 60.3% of accuracy. DF1 significantly ($H(2) = 15.9; p = 0.0004$) distinguished between young and middle-aged group ($p = 0.0002$) as well as between young and elderly groups ($p = 0.0032$) mostly on the basis of contrast between DMN and salience + control networks with younger subjects exhibiting lower metastability in DMN but higher metastability in salience, dorsal attention and control networks. DF2 significantly ($H(2) = 16.69; p = 0.0002$) discriminated between young and old groups ($p < 0.0049$) as well as between middle-aged and old group ($p = 0.0004$) with older subjects having higher metastability in dorsal and ventral attention networks but lower metastability in control and DMN. 5.7 captures rank-relationship between metastability of groups along the directions of DF1 and DF2.

The results of discriminant analysis suggest that there are two different combination of resting state network systems that are affected by age; each affected at the different point in lifespan. System ascribed to DF1 operates after the young age; during maturation and system described by DF2 operates at the old age, during the aging process.

Table 5.3: Wilk's Lambda

Test of Function	**Wilk 's Lambda**	**Chi-square**	**df**	**Sig.**
1	0.439	34.56	14	0.002
2	0.693	15.427	6	0.017

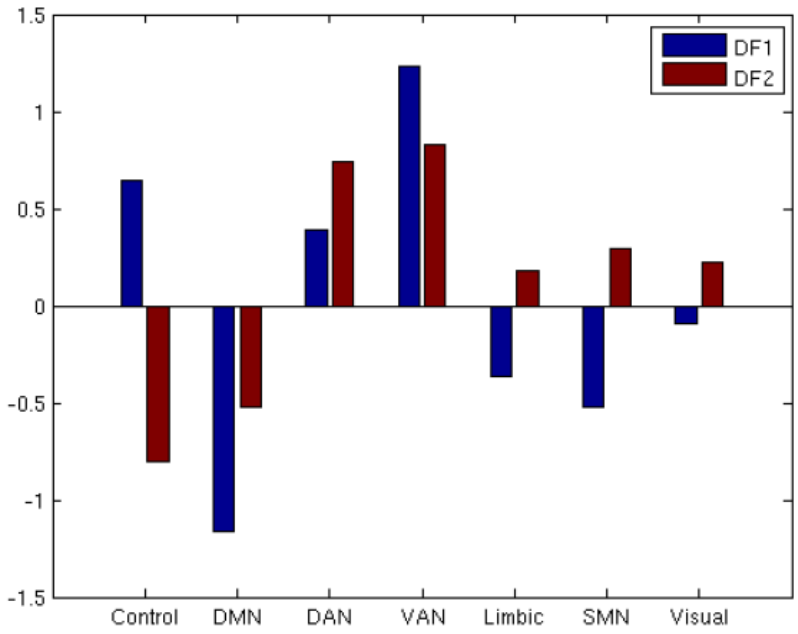

Figure 5.5: Loadings of each variable on two functions (DF1 and DF2) identified by DFA. DF1 largely reflects the previously reported well-known dichotomy between salience, control (task positive) and DMN (task negative) networks while DF2 captures interesting pattern with strong positive effects of Ventral and Dorsal attention network together with strong negative effects of Control and Default Mode Network.

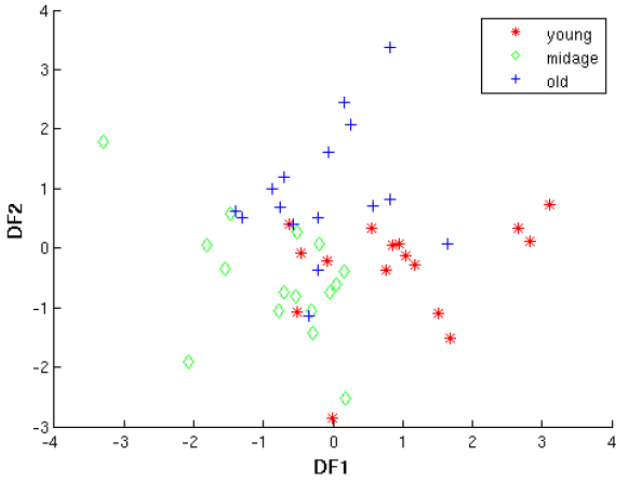

Figure 5.6: DF1 against DF2. 72.9 % (60.3% after leave-one out cross-validation) of original data-points were successfully classified. Elderly adults have higher variance along positive DF2 axis while young and middle-aged adults show higher variance along positive and negative DF1 axis respectively.

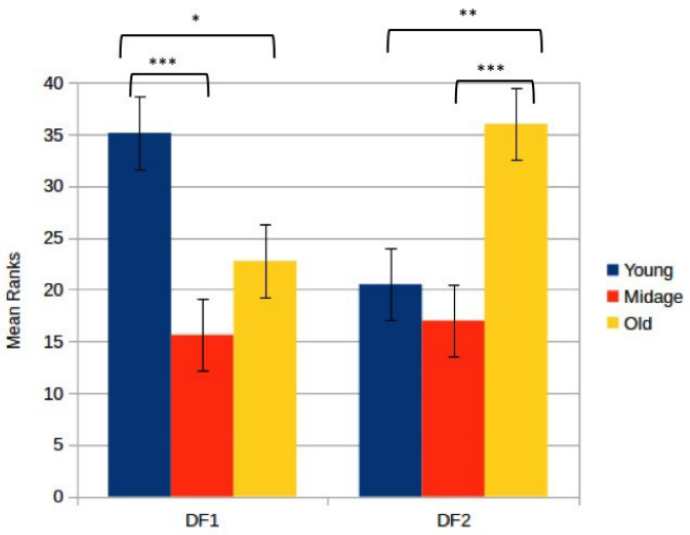

Figure 5.7: Comparison of mean ranks on DF1 and DF2 obtained from *post-hoc* multiple comparisons on results of non-parametric one-way ANOVA. *p <0.05, **p <0.005, ***p <0.0005

5.4 Discussion and Conclusions

We studied the effect of age on dynamic repertoire of the intrinsic activity of the brain. We evaluated metastability (i.e., the ability of BOLD signals of cortical regions to co-ordinate and compete in time [10]) across three uniformly distributed age groups: young, middle-aged and old. We found significant differences in whole-brain metastability between old and middle-aged groups suggesting that older participants are likely to visit more distinct 'states' at rest than the middle-aged participants. Yeo et al. [106] have shown that functional entropy of the resting state networks increases with age, suggestive of more spatially widespread correlation pattern with age. Our results partially confirm this finding in temporal domain suggesting that increased entropy in static-FC of elderly adults might be a result of the increased variability in dynamic FC. In contrast to their results, such effect was not significant between young to middle-age.

As discussed in Chapter 2, Battaglia *et al.* have shown that the fluctuation in dynamic FC becomes slower with age [91]. They used Pearson correlation coefficient to measure windowed FCs, considered age as a continuous variable and assessed properties of 'Jump Length Distribution (JLD)' of dynamic FC matrices to reach to this conclusion. At the first look, our results of higher metastability might seem to be in disagreement with this study but they are not. Battglia and colleagues explored the 'speed' of the FCD while here we indirectly studied the '(dis-)similarity' among the network-states explored. Battaglia and colleagues in a sub-analysis, studied the temporal stability of the modular structure of the dynamic FC networks and concluded that older adults showed lower temporal stability of FC networks (and hence, high average 'fluidity' in the

modular architecture) despite overall decrease in the speed of transition. Interestingly, this result complements ours, since we also find high variability in the way network nodes synchronize with each other (i.e., the way they define modules) in older adults.

Grady et al.[85] used partial least squares to assess age-effect on standard deviation of BOLD signals and confirmed wide-spread age-related patterns with some regions showing increased variability while others showing decease with age. However, the study contained only young and elderly groups. Our results show that more robust patterns of variability exist between young to middle-aged as well as middle-aged to old.

To understand the metastable behavior across topologically distinct functional networks, we use community detection algorithm on mean-FC and compared metastability of detected communities across age groups. We found significant difference between middle-to-old age groups only in one community, which contained regions from control network and ventral attention network. However, on applying multivariate discriminant analysis across networks show that richer age-related differences exist due to combined effects of these networks, which remain largely undetectable by considering only static mean-FC for graph theoretic analysis. We also find that default mode network does not show significant age-effects in the independent univariate analysis. However, when taken together with other networks, it does contribute to the predictability of age.

Most interesting results were obtained from the discriminant analysis. We found two different patterns of change in metastability each of which significantly discriminate between maturation (young to middle-age) and aging (middle-age to old) processes. Precisely, first pattern revealed higher metastability in control and attention systems with lower metastability of default mode, limbic and sensorimotor systems in young subjects compared to other two groups. Second pattern showed reversed pattern in metastability of control, limbic and somatosensory (SMN and visual) networks. Precisely, old subjects have significantly higher metastability in attention networks, limbic and sensorimotor networks while significantly lower metastability in control and default mode regions than that of other two groups. This observation confirms claims of default-executive coupling hypothesis in old age [70], which precisely suggests reduced segregation between default mode and executive control network. We provide additional evidence that increased coupling between these two systems is most likely due to reduced metastability of control network in old age. Most striking difference between maturation to aging process therefore can be attributed precisely to the reversed role of control network in terms of its significantly lower metastability. We speculate that process of maturation might gradually converge to the process of aging when the fronto-parietal control network decouples from the attention networks and couples with the default mode regions due to reduction in metastability of this network.

Chapter 6

Whole-brain Computation Modelling Approach

6.1 Introduction

In the previous chapter, we demonstrated the importance of investigating the metastability of BOLD signals to understand the age-effects on the resting state dynamics. Although characterizing the metastability of brain dynamics is the first step, and provides empirical support for our hypothesis, such investigations do not give information about the underlying dynamics that take place at faster timescales (e.g. firing rate/ oscillations of the local neural populations). Aging is a multifactorial process and understanding the system at multiple different spatiotemporal scales is warranted. Recent whole-brain computational modeling studies try to bridge this gap by modeling the dynamics of 'networks of networks' [57]. In these models, activity of each brain region (or node of our SC matrix) is modelled as biologically plausible (sometimes recurrent) network of neural populations and each of these networks is further connected according to the connectivity strengths obtained from the DTI tractography data (i.e., edge weights of our SC matrix). (See section 'Whole-brain Computational Models' in Chapter 1 for more details).

Fig. 6.1 explains the typical work-flow for these computational models. Depending on the local phenomenon that each model is trying to explain, several local parameters must be considered. For e.g., if we are interested in simulating firing rate of the excitatory and inhibitory neural population, we can consider rate coded network models or more realistic - conduction based spiking neural network [107, 108] [1] or neural mass model [109] at each node. If we are interested in simulating oscillatory behaviour of neural population, we can consider simple oscillators, Fitzhugh-Nagumo oscillators [110] or Kuramoto oscillators [59] as a local model at each node of SC. Each of these models has a number of parameters that need to be tuned at each SC node. Apart from the local network parameters, noise is added to the system and hence, the mean and standard deviation of the Gaussian noise is listed as one of the parameters in Fig. 6.1.

[1] http://kevin-gurney.staff.shef.ac.uk/files/Sem2/Lecture4/KG_comp_neuro_S2_L4_handout.pdf

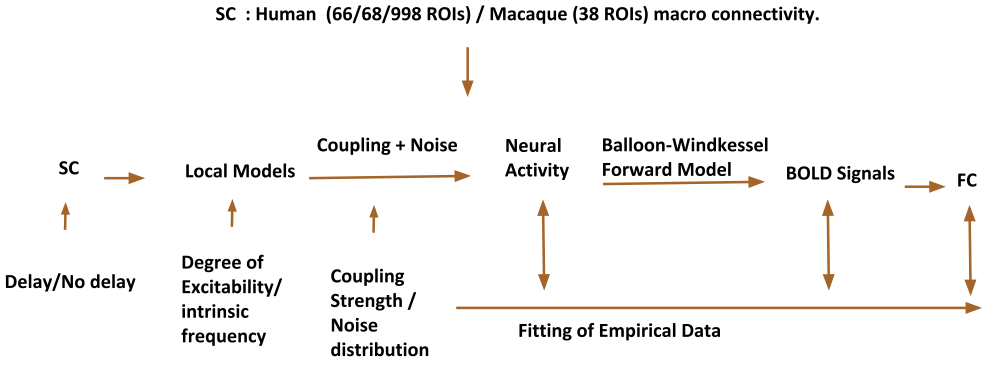

Figure 6.1: Typical work-flow for the whole-brain computational models. Input to this models is generally structural connectivity (SC) matrix and output is the time-series of neural activity of each node of SC. A forward model of Hemodynamic Response can be convolved with the neural activity to simulate slower BOLD signals that in turn can compute functional connectivity (FC) matrix. Free parameters at each step are shown in the bottom panel.

Optionally a conduction delay parameter can be used for each long-range connection between two SC nodes (i.e., an edge in SC matrix). The delay is typically calculated in terms of mean velocity (another free parameter to tune) and distance between two nodes as obtained from the DTI tractography data. Moreover, each SC connection is scaled by mean coupling strength (G), which is another free parameter which can control the effect of SC coupling. For e.g., if $G = 0$, all SC nodes are independent of each other and if $G = 1$ they are connected according to the actual SC edge weights.

The global parameters like mean velocity ($\sim$ mean delay) and global coupling strength (G) capture the changes in the qualitative behavior of the system. Hence, these parameters are known as 'control parameters'. For a specific range of values of control parameters, the behavior of the system resembles the empirical results, determining the 'dynamical working point' of the system. The most consistent result from the previous studies that simulate resting state neural activity is this: the working point of the system is obtained when the system is sub-critical i.e., close to the steady state solution.

The computational models have also previously shown how the shift in the working point occurs due to lesion (removal of a node in SC) or deterioration in the number of fibers (change of weights in edges of SC) because of disease [111, 112]. We hypothesized here that the network-level changes that occur with age are also due to similar shifts of the working point. These

models can systematically relate the micro-scale properties of the local dynamics (such as firing rates, time-delays, neural oscillations, synchronization, and metastability of neural signals) to the network-level dynamics (such as integration, segregation, functional connectivity dynamics, and multistability) [113]. Our proposition is that a small change in white matter fiber tracts that connect the dynamically important network nodes can result in a shift in the working point (the point at which the simulated FC best matches with the empirical FC) of a dynamical system.

To test our hypothesis, we carried out several simulation studies for the two existing whole-brain computational models- a simple attractor model with noisy fluctuations, named as the *Reduced mean field model* and an oscillator model with time-delay between the SC nodes, named as the *Kuramoto Model*. Before we give the details of each of these models, we will explain how the dynamics of the system defined by these models are related to the metastability using a toy example.

6.2 Theory

6.2.1 Parameter Space and Metastability – A Toy Example

Consider a dynamical system described by a state variable ϕ and control parameters $p1$ and $p2$ such that

$$\dot{\phi} = f(\phi(t), p1, p2)$$

then, $\dot{\phi}$ versus ϕ plot graphically represents the qualitative behavior of this system (For e.g., Fig. 6.2(a)). The 'fixed points' are created wherever $\dot{\phi} = 0$.

If the slope of the curve at fixed point is negative, the fixed point is stable, and it is called an attractor (represented as two closed dots in Fig. 6.2(a)). If the slope is positive, the fixed point is unstable (represented as open dots in Fig. 6.2(a)).

The choice of function f and values of control parameters p1 & p2 determine the behaviour of the dynamical system. In most cases, f is chosen such that the system exhibits 'local bifurcation' i.e., a small change in the parameter values ($p1$ and/or $p2$) causes a sudden 'qualitative' change in system behaviour.

Consider Fig. 6.2. This figure depicts the dynamics of the system defined by a normal form of the Haken-Kelso-Bunz (HKB) model [114]. This model was first used to theoretically explain the phase-transitions in the coordination of human hand-movements. However, without going into the details of this model, we can explain the various types of dynamics (attractor dynamics, metastability, or multistability) this system exhibits depending on the parameter values.

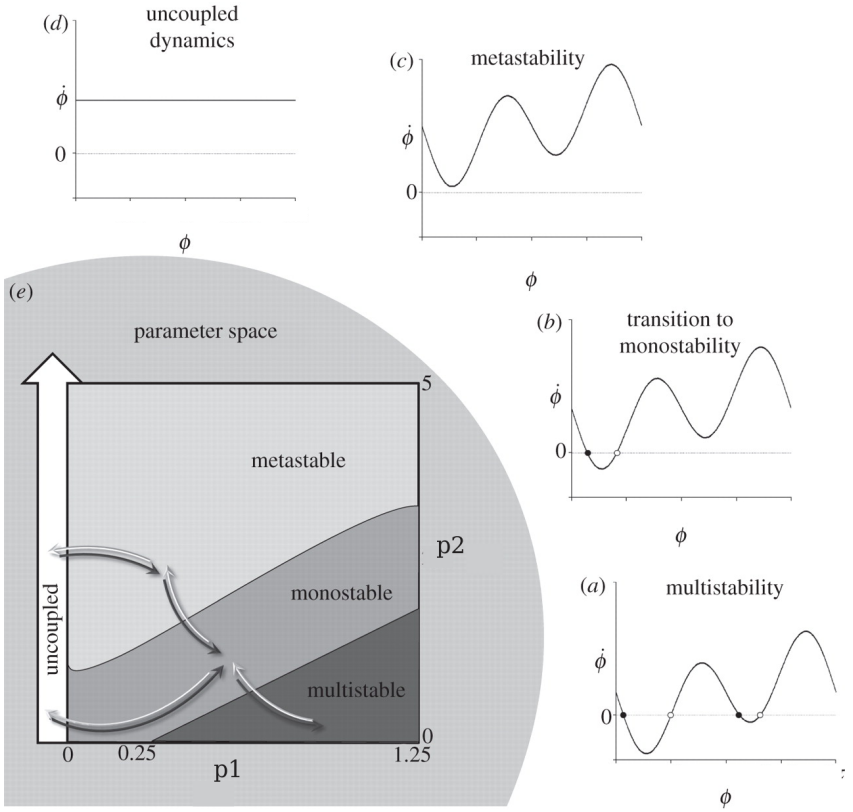

Figure 6.2: Example of bifurcation/ phase transitions. Figure adapted and modified from [9]

Fig. 6.2(E) represents the parameter space (or a phase diagram) of the system. i.e., the possible trajectories of the system as a function of control parameters $p1$ and $p2$. Four kinds of dynamics are possible in this case. For any value of $p2$, if $p1 = 0$, the system has constant rate of change (i.e. $\dot{\phi} = c, c \in \mathbb{R}$) (Fig. 6.2 (d)). If $0 < p1 < 0.25$ and the system can either be in monostable (Fig. 6.2 (b)) or metastable (Fig. 6.2(c)) regime depending on the value of $p2$. For higher values of $p2$, the system is metastable, i.e., it is close to the attractor, but since there are no fixed points, system never reaches the steady state. As we keep decreasing value of $p2$ while keeping $p1$ the same, two new fixed points are created (Fig. 6.2 (b)), out of which one is stable. Hence, the system always settles down in this state and is said to be in *monostable regime*.

For $0.25 < p1 < 1.25$, there are two possible transitions depending on values of $p2$ – monostability and multistability. As we further decrease the value of $p2$, the system transitions into multistability (or bistability, to be precise). That is, two new fixed points are created and now there are two attractors (Fig. (6.2 (a)). The system can settle into any of these attractor states depending on the initial values.

To conclude, control parameters divide the phase-space into three different regimes (Fig. 6.2 (e)). Transition from any regime to any other regime is known as *bifurcation* or *phase-transition*. Phase-transitions are common in case of complex biological systems such as in brain and be-

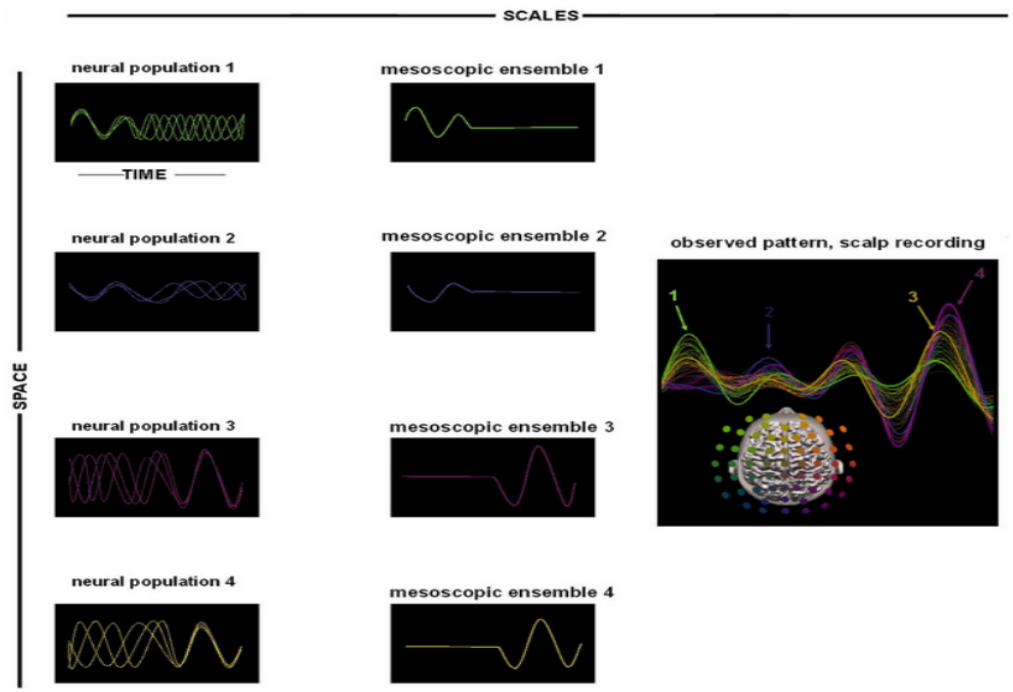

Figure 6.3: Neural Dynamics observed at different spatiotemporal scales. Phase alignment in the metastable dynamics at the microscopic scale can be reflected in state-transitions (multistable) dynamics at the mesoscopic and macroscopic scales. Figure adapted from [10]

haviour. The metastable and multistable behaviours are interesting in particular for resting state dynamics because empirical data suggests a rich dynamic repertoire (e.g., many different possible configurations of FC in time). Such rich dynamics are possible only within the regime of metastability and multistability. And that is why the dynamical working point (that explores resting state dynamics) of the whole-brain computational models is always located at the edge of criticality in the metastable or multistable regime.

Another interesting property of the brain dynamics is the ability to exhibit different dynamics at different scales. This phenomenon is depicted in Fig. 6.3. Left most panel shows oscillations from four neural populations. Each individual neuron-pair can be in metastable regime (i.e., synchronizing and desynchronizing transiently) or they might show epochs of coherence. If the mesoscale signal is recorded, only the epochs where phases are aligned will be captured, leaving out the epochs where phases cancel each other (central panel). Hence, the observed dynamics at the mesoscale will be in multistable regime. However, at the macro-scale (e.g., recording of EEG here), many such sources will be considered and the dynamics of this system can be modeled as metastable system. Again, if we consider FC that represents pairwise coherence between each of these sources, the dynamics of FC can be modeled in terms of state-transition or multistable dynamics. Due to this scale-invariance, local dynamics of the nodes in the whole-brain computational model can be described at any level of investigation to explore age-related

shift in the dynamical working point. Here we used two such models (at each node of SC) at different levels of description. Next we explain these models and the computational methods used to carry out simulations.

6.3 Methods

6.3.1 Reduced Dynamic Mean Field (DMF) Model

The DMF model [18] is biologically detailed, mathematically derived from the most realistic spiking neuron models, simulates firing rate of the neural populations of excitatory neurons and has the attractor dynamics, hence DMF can exhibit either monostability or multistability.

The dynamics of this model can be expressed as the passive decay differential equation of the Synaptic gating variable (S) along with the noisy Gaussian fluctuations (equation 6.1). Firing rate is approximated based on the Sigmoid (transfer) function of the total synaptic input current (equation 6.2). The dynamics of each local network of excitatory and inhibitory populations of spiking neurons interconnected via long-range excitatory synapses can be expressed by a single one-dimensional differential equation 6.1. The global brain dynamics of the network of interconnected local networks can be described by the following set of equations [18]:

$$\frac{dS_i}{dt} = -\frac{S_i}{\tau_S} + (1 - S_i))\gamma H(x_i) + \sigma\nu_i(t) \tag{6.1}$$

$$H(x_i) = \frac{ax_i - b}{1 - exp(-d(ax_i - b))} \tag{6.2}$$

$$x_i = wJ_N S_i + GJ_N \sum_j C_{ij} S_j + I_0 \tag{6.3}$$

Here S_i is a synaptic gating variable of area i and is the state variable. The kinetic parameters are $\gamma = 0.641/1000$, and $\tau_S = 100$ ms. H is the non-linear sigmoidal input-output transfer function. parameters $a = 270(nC)^{-1}$, $b = 108Hz$ and $d = 0.154s$ control the non-linearity of the sigmoidal curve. x_i is the total synaptic input current at the afferent node i. $J_N = 0.2609nA$ is the synaptic coupling or gain. $w = 0.9$ is connection strength of intra-network excitatory connections. G is inter-network coupling strength and is a control parameter. C_{ij} represents entries of the SC matrix that captures the structural connectivity between regions i and j. $I_0 = 0.3nA$ is the constant external input current. ν_i in Equation (6.1) is uncorrelated standard Gaussian noise with noise amplitude $\sigma = 0.001nA$. Detailed derivation of the reduced DMF equations and description of each of these parameters is given in Deco *et al* [18]. Parameter values were chosen as per the original paper except each of the values is scaled such that the

control parameter G can be explored in the range of 0 to 1. (Abbreviations: nA= nanoampere, nC= nanocoulomb)

The stochastic differential equation (SDE) system was solved numerically using Euler-Maruyama [115] method with step size of 1. This method generalizes Euler's integration scheme for SDEs by integrating the noise term as a standard Wiener process. Synaptic activity ($S_n = 0$ if $S < 0$ and 1 if $S > 1$) and firing rate ($H(x)$) were simulated at each time-step for total of $4 \times 60 \times 1000(ms)$ (=4 mins).

To simulate the BOLD signals from neural activity, forward Balloon-Windkessel model was used [116]. This model assumes that the BOLD signal is a static nonlinear function of the normalized total deoxyhemoglobin voxel content, normalized venous volume, resting net oxygen extraction fraction by the capillary bed and resting blood volume fraction. The model is described by the four coupled nonlinear differential equations as described in [18]. Euler's method (ODE45) was used with step size of 0.001 to numerically solve this system. The BOLD activity was further down-sampled to 2s to match the TR of empirical data. Moreover, data from first 500ms were removed to ensure stabilization of the dynamics.

6.3.2 Two-Dimensional Oscillator - Kuramoto Model

The second model, Kuramoto model is biologically less detailed, but exhibits richer dynamics than the DMF model. It simulates instantaneous phases of the oscillations in neural populations, has oscillatory dynamics and can exhibit metastability. The local oscillatory dynamics at each node of SC matrix can be described as follows:

$$\frac{d\theta_n}{dt} = \omega_n + k \sum_{p=1}^{N} C_{np} sin(\theta_p(t - \tau_{np}) - \theta_n(t)) + \eta_n(t), n = 1, \cdots, N \tag{6.4}$$

where θ_n is the phase of the oscillator at node n and a state variable, $\omega_n = 2\pi f$ is the intrinsic angular frequency. The intrinsic frequency (f) at each node was chosen from a Gaussian distribution $N(\mu, \sigma) \sim (40, 3)$. k is the global coupling strength, that is similar to the parameter G from the previous model. Since k controls the effect of structural connectivity on the overall outcome, it is known as control parameter. I.e., if $k = 0$, all oscillators are independent, for $k = 1$, all of them will be coupled according to their structural connectivity (SC). C_{np} is an entry from SC matrix representing SC strength between nodes n and p. $\tau_{np} = L_{np}/V$ is the *instantaneous* conduction delay between the nodes n and p. Where L_{np} is entry from the distance matrix as defined in chapter 3 (figure 3.4 left panel). It determines the mean aggregate distance between node n and p (and is different from SC). V is mean velocity which is defined as follows: $V = \langle\tau\rangle L_{np}/\langle L\rangle$. Where $\langle L\rangle$ is the average distance i.e. mean of the all the entries in the distance matrix. $\langle\tau\rangle$ is the *average* conduction delay and another control parameter (free

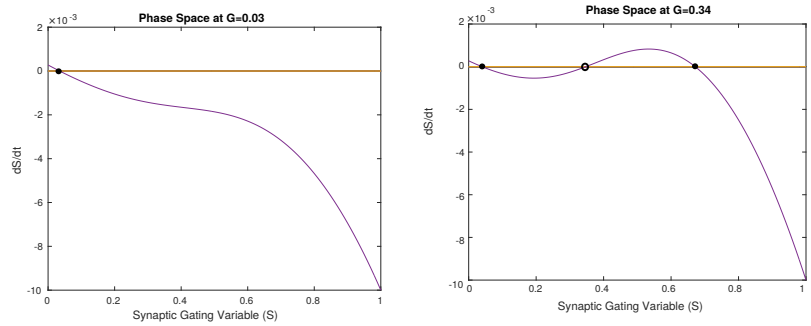

Figure 6.4: Saddle-node bifurcation with increase in coupling strength G. For example, at G=0.03, system exhibited monostability while for G=0.34, system showed bistability.

parameter) of the system. $\eta_n(t)$ is a noise term with Gaussian random distribution with 0 mean and standard deviation of $\sigma/\sqrt{T}$. Detailed discussion on parameter selections can be found in [59].

First we explored the parameter space of τ and k for the three age-groups. Three group averaged mean SC matrices (for young, middle-age and old) and three distance matrices were used for this analysis. Eq. 6.4 was numerically integrated using the same Euler-Maruyama method with a step size of 0.01 ms and for a duration of 800s. The instantaneous phases were further converted to a neural signal as $r_n = sin(\theta_n(t))$ for each node n. The simulated activity was further down-sampled by the factor of 100 such that the data is saved in ms resolution. BOLD activity was calculated from this neural activity as explained in the previous section. The results of each of which can be explained as follows.

6.4 Preliminary Results

6.4.1 Reduced Dynamic Mean Field (DMF) Model

Due to its simplicity, one-dimensional attractor DMF model could be used for bifurcation analysis. We began with plotting $\dot{S}$ *vs* S for various values of coupling strength (G). As the coupling strength increased, new fixed points were created and dissolved. Hence, the system showed saddle-node bifurcation. Two representative trajectories are shown in Fig. 6.4. For G=0.03, there was only one attractor point at S=0.02. For G=0.34 however, new attractor emerged at around $S \sim 0.7$ and the system became bistable. Note that this dynamics is representative of the deterministic system (without adding noise) and for each individual area network (disregarding the SC couplings).

To understand the bistability in more realistic setting, we simulated neural activity and firing rate for T=5000ms for the mean SC averaged across all subjects (N=68) and with added noise

$\sigma = 0.001$ as in [17]. We simulated the model at each of the 1000 equidistant points between $0 < G < 1$ and obtained $N \times T$ matrix representing firing rate of each 68 nodes (ROI). To visualize the data, we applied Principle Component Analysis (PCA) on this $N \times T$ matrix and reduced the dimensionality to two Principle Components (PC). Transforming these two PCs back to the native space, we found the maximum firing rates for each component at each iteration. This is shown in Fig. 6.5(A). Notice that for $G < 0.197$, both the components showed maximum firing rate ($x < 5$ Hz), suggesting that all 68 regions achieved very low-firing rate (monostability). However, in the bistability regime ($\sim 0.2 < G < 0.45$), there were two major components, one set of regions achieved firing rate close to 20Hz, while the others achieved a high firing rate close to 40-80Hz. These firing rates are biologically realistic and match the firing rates of neural populations during rest – hence, validating the model for our data. 6.5(B) and 6.5(C) shows the time-evolution of synaptic gating variable and firing rates of each N=68 regions for G=0.25, in bistable regime.

Next, we simulated the neural activity for $T = 4 \times 60 \times 1000$ ms to also generate BOLD signals and FC using pairwise Pearson correlation. For each individual SC matrices, the simulation was run for 1000 random G values obtained from standard uniform distribution, and model accuracy was obtained in terms of Pearson Correlation Coefficient between simulated and empirical FC. These results are shown in Fig. 6.6. Only the mean accuracy of each age-group is plotted here for better visualization. As we have defined earlier, the dynamical working point of this system can be obtained at $\sim G > 0.4$. since the accuracy suddenly increases at this point. Interestingly enough, this point lies on the edge between the bistability and multistable regime where the firing rate of all regions are very high (see Fig. 6.5(A)).

This result directly supports our hypothesis of the shift in dynamical working point for the elderly adults. In Fig. 6.6, the fitting curves for elderly are slightly shifted rightward starting from the bistable regime than the other two groups. This effect became prominent in the very high firing rate regime (for $G >> 0.4$).

Next, to understand the age effect on the shift more clearly, accuracy was plotted for each subject in Fig. 6.7 for $G = 0.4$. As shown, the accuracy of the model decreased as a function of age ($r = -0.46$), suggesting that the dynamics of the resting brain becomes less predictable with age.

6.4.2 Kuramoto Oscillator Model

Next, to directly investigate the metastability and to understand the effect of long-range conduction delays on the model, we simulated the Kuramoto model at each node.

The neural activity was simulated for the range of control parameter values $(k, \langle\tau\rangle) = (0.01 : 0.01 : 1, 0.1 : 0.1 : 10)$ for the three mean SC matrices averaged across participants in each age-

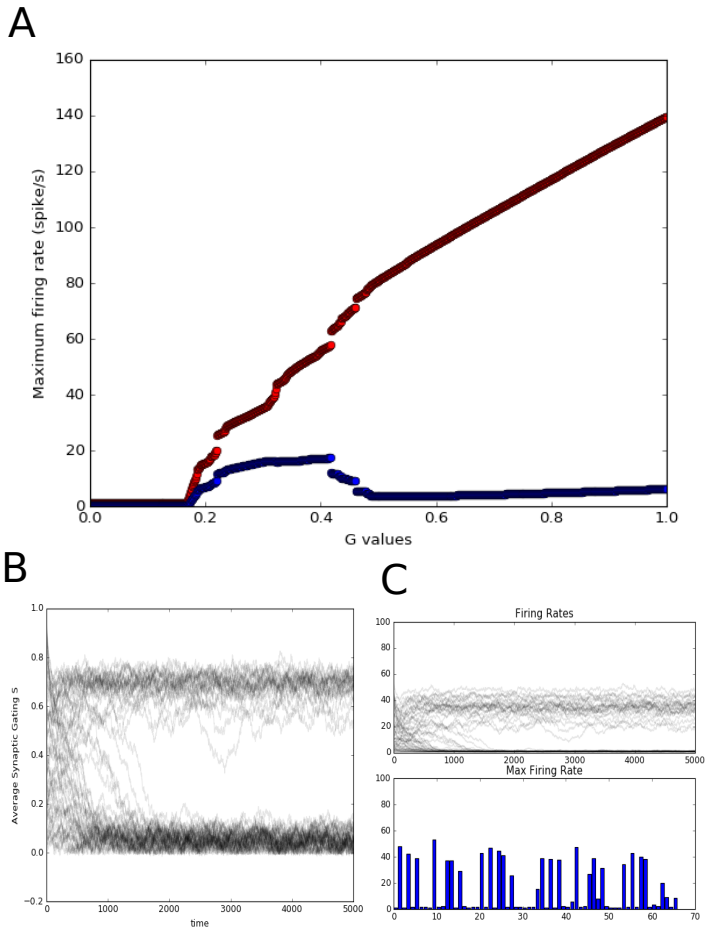

Figure 6.5: Relationship between coupling strength and firing rates of each regions. (A) The bifurcation plot of the system defined by Eq. 6.1-6.3. The bifurcation was realized as synaptic activity of each N=68 regions (in B) and firing rates (C)(top panel) of these regions at $G = 0.25$. The maximum firing rate achieved by each regions is shown in bottom panel.

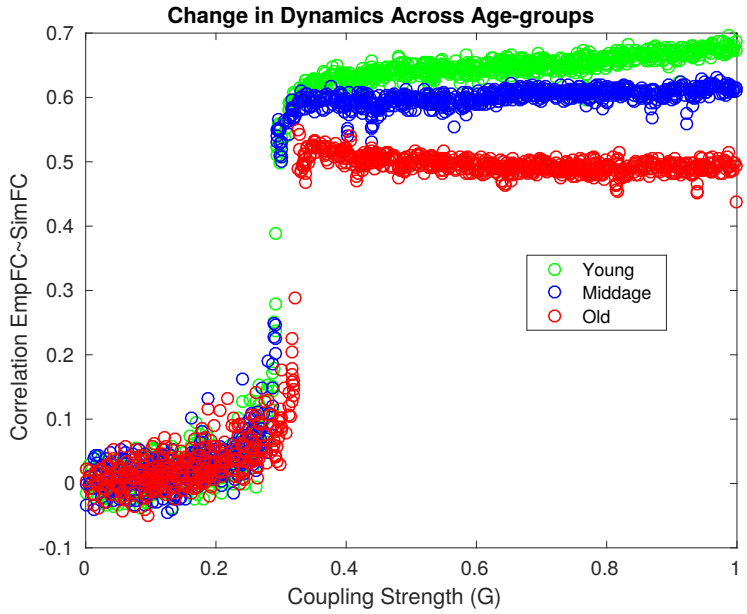

Figure 6.6: Accuracy of models (Pearson correlation between empirical and simulated FCs) for each 1000 random values of G. Only the mean accuracy values are shown for each age-group for better visualization. Note the rightward shift in the dynamical working point of elderly adults compared to the other two groups.

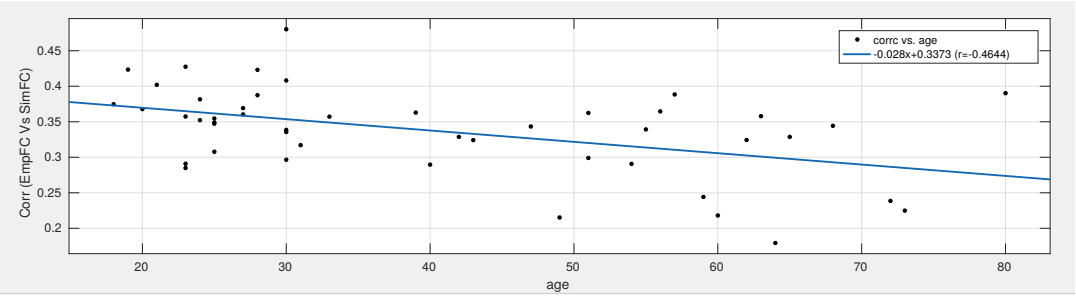

Figure 6.7: The model accuracy (fitting between empirical and simulated FC) decreased as a function of age for the fixed value of control parameter $G = 0.4$, suggesting that dynamic coupling between SC-FC reduces with age.

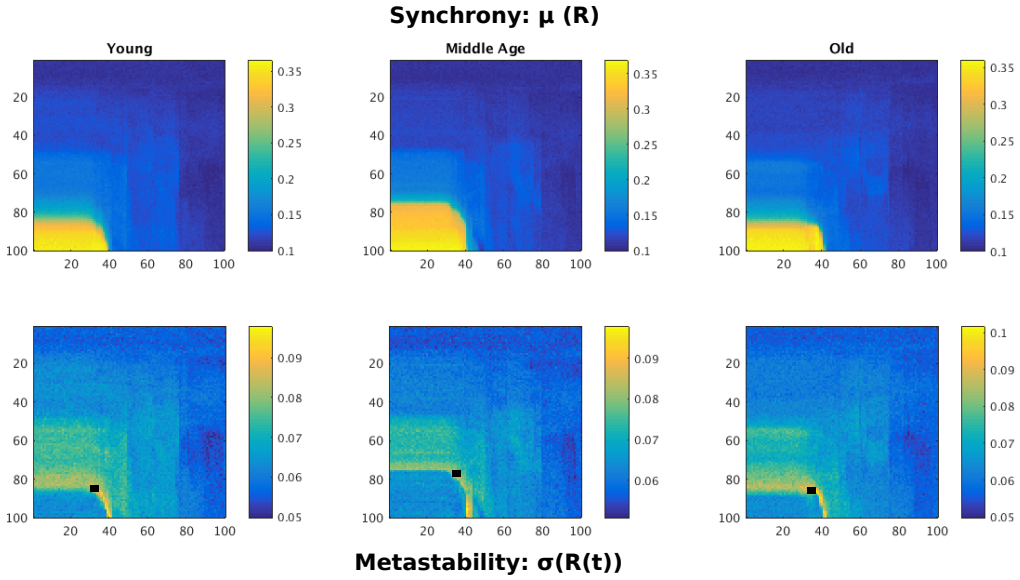

Figure 6.8: Parameter space for the model explained in Eq. 6.4 for the three age-groups. Top Panel shows synchrony (mean of Kuramoto Order Parameter, R) and Bottom Panel depicts metastability (SD of R) for each of the 100×100 parameter value pairs of mean coupling strength (k) on the X-axis and mean conduction delay ($\langle\tau\rangle$) on the Y-axis. The point of highest metastability for each group is indicated with black dot in the bottom panel.

group. For each of these iterations, synchrony and metastability were calculated in the same way as defined in Chapter 5, but this time using the simulated instantaneous phases rather than the actual data. Kuramoto order Parameter (R) was defined as in 5.2, however instead of phases of BOLD signals, ϕ, we can now use the simulated instantaneous phases θ obtained from 6.4. Synchrony was estimated as a mean of Kuramoto Order Parameter across all regions i.e. $\mu(R)$ and metastability is defined as the standard deviation of Kuramoto Order Parameter ($\sigma(R)$). Fig 6.8 depicts the differences in synchrony and metastability values in the parameter space of $(k, \langle\tau\rangle)$ for the three age-groups. As seen, the two control parameters divided the parameter space into three different regimes of very low synchrony, very high synchrony and moderate synchrony among the $N = 68$ regions of the brain. The metastability was highest in the moderate synchrony regime and lower in the very high or very low synchrony regimes for all the three mean age-groups. There were seemingly qualitative differences among the three age-groups. For e.g., the high synchronous regime for the young and elderly mean were skewed towards the higher coupling strength (k) values, suggesting a rightward shift that was observed in the previous section. Moreover, the higher metastability regime of elderly adults extended till the even higher values of mean conduction delay parameter, as compared to middle-aged group. Suggesting a downward shift in the dynamics due to mean delays between the white matter fiber connections. Overall the metastability values were higher for elderly adults than the other two groups.

6.5 Discussion & Conclusions

We simulated the neural activity as a function of the underlying population firing rate (in DMF model) and a function of the instantaneous phase (in Kuramoto model) of the neural oscillations. In both the cases, our purpose was to understand the effect of aging on these microscopic properties of the brain and whether or not the models can simulate the change in working point of the system with age.

6.5.1 DMF Model

We first replicated the PCA results from [17] for our aging dataset and found that the system of these $N = 68$ coupled regions exhibits the same bifurcation properties as in the original study. However, when the DMF model is simulated for each individual with the same parameters, the accuracy of the model fit (approximated across 1000 odd iterations) for elderly adults is seemingly different than the other two groups in the high firing rate regime of the system. This result supports the empirical evidence that suggests that the BOLD signal variability of the elderly adults might be due to abnormally high firing of the excitatory population across many connected regions [117, 85]. The lower accuracy result for the elderly adults also points towards the decreasing SC-FC coupling with age, which was previously shown using empirical results by [5]. Interestingly we observed a slightly rightward shift in the accuracy curve of elderly suggesting that, elderly adults required higher coupling strength among the neural populations to generate the FC similar to that observed in the patients with Parkinson's disease. However, the shift was not very prominent and better simulation experiments are required to design before we can comment on these results. In our simulations, the noise-level was kept constant for each subject. In future, the effect of noise on the dynamical working point can be evaluated by comparing the models with and without noise. This can also be helpful in evaluating the effect of noise on multistability of the system of elderly adults.

6.5.2 Kuramoto Model

Kuramoto model, having an oscillator dynamics, does not settle into a stable state but remain in perpetual state of oscillation where the instantaneous phases constantly change. Hence, for a particular range of control parameters, the model can remain metastable. Hence, Kuramoto model was used to directly investigate the metastability of neural signals and to understand the effect of mean delay between the long range connections and coupling strength. The preliminary results showed qualitative differences in synchrony and metastability of neural signals of elderly adults compared to middle-aged adults. This result is particularly interesting since it directly validates the previous empirical results obtained from the BOLD signals. As discussed in the

'Theory' subsection, this is an example of a typical case where the neural signal as well as BOLD signals both showed higher metastability in case of elderly adults suggesting that the BOLD signal variability has neural origin.

One interesting result in particular is the common effect of delay and coupling strength on the synchrony and metastability of the elderly. For the mean delay values in the bio-physically valid range of 8-10 ms, the whole-brain synchrony of elderly adults was lower than that of middle-aged subjects but metastability was higher than that of elderly. These results suggest that at least the part of the higher metastability observed at BOLD signal level of elderly adults is due to increased conduction delays in long-range connections. The delays might be due to demyelination of the white-matter fiber bundles which is a common observation in the aging literature. Again, a rightward shift in the coupling strength was observed only for the range of 8-10ms delay in elderly adults compared to middle-aged, suggesting that the combined effect of demyelination and decrease in white-matter fiber strength can be the reason for the change in the dynamics of the elderly adults and thus in the metastability of neural and BOLD signals. However, these intuitions are based on the visual inspection of the parameters. In future more rigorous methods are required to be used to quantitatively analyze the effect of age on these parameters and eventually on the resting state dynamics of the system.

Chapter 7

Conclusions and Future Work

All thoughts and cognitive operations emerge from the stream of consciousness – a widely held belief in the Western and the Eastern philosophies. In the context of the observable brain dynamics, there is no permanent state of the brain that sustains across the lifespan. The complexity of dynamic processes of the brain in aging is better understood and with certainly greater clarity using the concept of metastability, in other words the ability of the system to transition between different cognitive states. Aging is not a state but a process that continuously unfolds in time, leading to our proposed dynamic hypothesis of aging. As a person grows older, top-down influences due to training and new learning continuously shape the steady-state dynamics of the brain. Concomitantly, bottom-up changes at the genetic, molecular, and neural levels as a result of age will affect the structure of the brain. Hence, age-related changes should be understood as being merely another dynamic process that takes place as a result of changes in a metastable system that operate at a smaller spatiotemporal scale. The age-related changes that are observed in the phase synchronization of various networks and functional connectivity dynamics (FCD) are one of the first markers available to understand the combined effects of age-related structural changes and the change in the dynamics of the system, in other words, a shift in the dynamical working point of brain information processing as a function of age. However, data-driven methods alone are not sufficient for understanding the shift of working point. Personalized whole-brain computational models that can simulate FCD from the underlying neuronal dynamics of different brain regions will be necessary to track the change in the dynamical working point of the system.

In this thesis, we gave a comprehensive account of the theoretical, empirical and computational methods that can be used to investigate age effects on the dynamics of the brain. Here we chose resting state dynamics in particular because it is known to have the richest and intrinsic dynamics of all cognitive and brain states that the human brain can exhibit. It is also well-suited for understanding structure-function relationship since the dynamics at rest is assumed to be

solely an outcome of the physical processes that take place at different scales on the landscape of the structural topology.

This thesis contributed towards the research in two ways: (i) in the empirical study described in Chapter 5, we explored age-effect on the dynamic interactions between resting state functional networks. We found significant differences in whole-brain metastability of old adults than that of middle-aged. We also found changing role of functional network systems in terms of their metastability across age groups. This empirical investigation for the first time showed that the metastability of resting state networks could discriminate between the healthy young, middle-aged and older adults with higher accuracy, suggesting the role of network level variability in the investigation of aging studies.
(ii) In the computational study described in Chapter 6, we showed that the dynamical working point of the elderly adults significantly changes from middle-to old age. This shift in the working point is related to the increase in metastability in elderly adults suggesting the role of structural deterioration in changing the resting state dynamics in elderly adults. In both empirical and computational investigation, one point emerged very clearly that *although subtle local differences exist between young to middle age, the global properties of the brain (accommodating the whole-brain interactions) are significantly different only across middle-to-old age.* This result points towards a critical age which separates maturation and senescence.

One notable limitation of this study is the cross-sectional nature of investigation. Maturation and senescence are continuous processes affected by many other factors and cross-sectional studies cannot account for the intra-individual variability that exists due to genetic, molecular, neural and environmental differences. Therefore test-retest validation of the results proposed here in a longitudinal cohort study with appropriate phenotyping is required. How change in metastability is manifested at behavioral level is not yet well known. One might therefore consider similar analysis in task-based experimental setting and correlate metastability scores with the performance of elderly adults on various behavioral tests to understand whether the increased metastability of elderly adults is a beneficial or a detrimental process.

Studies have started using FCD as a proxy measure for understanding the metastability in the brain [118]. Even though there are no shortcut standard ways to defining metastability, better and better methods are being employed since the inception of this thesis 3 years back. K-means clustering algorithms to characterize stable “state" network patterns that are repeatedly explored in time, Markov processes for modeling FCD states can be used for extracting more information from the signals than presented in this thesis. Statistics such as the transition probability (i.e., the probability of transitioning from one state to another) and the dwell-time (i.e., the time spent by the subject in the states) can be used to characterize the network dynamics. On the computational front, we presented very preliminary results. Similar to lesion studies, the effect of removing edges or weakening selected edge-weights can be systematically studied.

At the end, the benefits of invoking the concept of metastability to understand aging are multifold: metastability provides us with a glimpse of the earliest age-related neural changes taking place when the brain reaches a steady-state after maturation. Second, this approach allows comparison of dynamical working points of high-performing and low-performing elderly adults, and that might explain the inter-individual variability often reported in aging-related studies. The third and most important outcome is that the combination of the theoretical framework of metastability and biologically-realistic whole-brain computational models might, for the first time, offer a coherent and unifying testable account of most of the changes observed in aging-related studies at different spatiotemporal scales. Although we have presented examples from the macroscopic brain imaging perspective in support of the existence of metastability in senescence, equally potent exemplars can be construed from the genetic and cellular mechanisms that underlie the processes of aging.

Publications

Thesis-Related Publications

- Naik S, Banerjee A, Bapi RS, Deco G, Roy D. Metastability in Senescence (2017). *Trends in Cognitive Sciences.* DOI: http://dx.doi.org/10.1016/j.tics.2017.04.007
- Naik, S., Subbareddy, O., Banerjee, A., Roy, D., & Bapi, R. S. (2017, May). Metastability of cortical BOLD signals in maturation and senescence. In Neural Networks (IJCNN), 2017 International Joint Conference on (pp. 4564-4570). IEEE. DOI: 10.1109/IJCNN.2017.7966435
- Surampudi, S. G., Naik, S., Shrama, A., Bapi, R. S., & Roy, D. (2016). Combining Multiscale Diffusion Kernels for Learning the Structural and Functional Brain Connectivity. bioRxiv, 078766. (Submitted)

Other Conference Articles

- Naik S., Pramod S.K., Shailesh Jain, Dipanjan Roy, & Raju S. Bapi *"Exploring Structural and Functional Connectivity in Autism Spectrum Disorder"* Short Paper presented at ACCS (2016), IIT Gandhinagar
- Naik S, Vattikonda A, Roy D., Bapi RS Age dependent Causality changes in Cortical Hubs over Lifespan. Abstract accepted at 3rd International Conference on Cognition, Brain and Computation (CBC, 2016), IIT Gandhinagar
- Shailaja Mekala, Vani B, Naik S., S Alladi *et al. "Neural basis of Cognitive Reserve in Ageing"* Abstract accepted at ACCS (2016), IIT Gandhinagar

Bibliography

[1] Olaf Sporns. The human connectome: a complex network. *Annals of the New York Academy of Sciences*, 1224(1):109–125, 2011.

[2] Richard F Betzel, Lisa Byrge, Ye He, Joaquín Goñi, Xi-Nian Zuo, and Olaf Sporns. Changes in structural and functional connectivity among resting-state networks across the human lifespan. *Neuroimage*, 102:345–357, 2014.

[3] Alistair Perry, Wei Wen, Anton Lord, Anbupalam Thalamuthu, Gloria Roberts, Philip B Mitchell, Perminder S Sachdev, and Michael Breakspear. The organisation of the elderly connectome. *Neuroimage*, 114:414–426, 2015.

[4] David Meunier, Sophie Achard, Alexa Morcom, and Ed Bullmore. Age-related changes in modular organization of human brain functional networks. *Neuroimage*, 44(3):715–723, 2009.

[5] Joelle Zimmermann, Petra Ritter, Kelly Shen, Simon Rothmeier, Michael Schirner, and Anthony R McIntosh. Structural architecture supports functional organization in the human aging brain at a regionwise and network level. *Human brain mapping*, 37(7):2645–2661, 2016.

[6] Rahul S Desikan, Florent Ségonne, Bruce Fischl, Brian T Quinn, Bradford C Dickerson, Deborah Blacker, Randy L Buckner, Anders M Dale, R Paul Maguire, Bradley T Hyman, et al. An automated labeling system for subdividing the human cerebral cortex on mri scans into gyral based regions of interest. *Neuroimage*, 31(3):968–980, 2006.

[7] Michael Schirner, Simon Rothmeier, Viktor K Jirsa, Anthony Randal McIntosh, and Petra Ritter. An automated pipeline for constructing personalized virtual brains from multimodal neuroimaging data. *Neuroimage*, 117:343–357, 2015.

[8] BT Thomas Yeo, Fenna M Krienen, Jorge Sepulcre, Mert R Sabuncu, Danial Lashkari, Marisa Hollinshead, Joshua L Roffman, Jordan W Smoller, Lilla Zöllei, Jonathan R Polimeni, et al. The organization of the human cerebral cortex estimated by intrinsic functional connectivity. *Journal of neurophysiology*, 106(3):1125–1165, 2011.

[9] JA Scott Kelso. Multistability and metastability: understanding dynamic coordination in the brain. *Phil. Trans. R. Soc. B*, 367(1591):906–918, 2012.

[10] Emmanuelle Tognoli and JA Scott Kelso. The metastable brain. *Neuron*, 81(1):35–48, 2014.

[11] Yoo Young Hoogendam, Albert Hofman, Jos N van der Geest, Aad van der Lugt, and Mohammad Arfan Ikram. Patterns of cognitive function in aging: the rotterdam study. *European journal of epidemiology*, 29(2):133–140, 2014.

[12] Fernanda Cabral Soares, Thaís Cristina Galdino de Oliveira, et al. Cantab object recognition and language tests to detect aging cognitive decline: an exploratory comparative study. *Clinical interventions in aging*, 10:37, 2015.

[13] Denise C Park, Gary Lautenschlager, Trey Hedden, Natalie S Davidson, Anderson D Smith, and Pamela K Smith. Models of visuospatial and verbal memory across the adult life span. *Psychology and aging*, 17(2):299, 2002.

[14] K Warner Schaie and Sherry L Willis. The seattle longitudinal study of adult cognitive development. *ISSBD bulletin*, 57(1):24, 2010.

[15] Jessica S Damoiseaux. Effects of aging on functional and structural brain connectivity. *NeuroImage*, 2017.

[16] Shruti Naik, Arpan Banerjee, Raju S Bapi, Gustavo Deco, and Dipanjan Roy. Metastability in senescence. *Trends in Cognitive Sciences*, 2017.

[17] Gustavo Deco, Viktor K Jirsa, and Anthony R McIntosh. Emerging concepts for the dynamical organization of resting-state activity in the brain. *Nature reviews. Neuroscience*, 12(1):43, 2011.

[18] Gustavo Deco, Viktor K Jirsa, and Anthony R McIntosh. Resting brains never rest: computational insights into potential cognitive architectures. *Trends in neurosciences*, 36(5):268–274, 2013.

[19] CJ Honey, O Sporns, Leila Cammoun, Xavier Gigandet, Jean-Philippe Thiran, Reto Meuli, and Patric Hagmann. Predicting human resting-state functional connectivity from structural connectivity. *Proceedings of the National Academy of Sciences*, 106(6):2035–2040, 2009.

[20] Enrique CA Hansen, Demian Battaglia, Andreas Spiegler, Gustavo Deco, and Viktor K Jirsa. Functional connectivity dynamics: modeling the switching behavior of the resting state. *Neuroimage*, 105:525–535, 2015.

[21] Gustavo Deco and Morten L Kringelbach. Metastability and coherence: Extending the communication through coherence hypothesis using a whole-brain computational perspective. *Trends in neurosciences*, 39(3):125–135, 2016.

[22] E Damaraju, EA Allen, A Belger, JM Ford, S McEwen, DH Mathalon, BA Mueller, GD Pearlson, SG Potkin, A Preda, et al. Dynamic functional connectivity analysis reveals transient states of dysconnectivity in schizophrenia. *NeuroImage: Clinical*, 5:298–308, 2014.

[23] Marion Sourty, Laurent Thoraval, Daniel Roquet, Jean-Paul Armspach, Jack Foucher, and Frédéric Blanc. Identifying dynamic functional connectivity changes in dementia with lewy bodies based on product hidden markov models. *Frontiers in Computational Neuroscience*, 10, 2016.

[24] Marcus E Raichle, Ann Mary MacLeod, Abraham Z Snyder, William J Powers, Debra A Gusnard, and Gordon L Shulman. A default mode of brain function. *Proceedings of the National Academy of Sciences*, 98(2):676–682, 2001.

[25] Malia F Mason, Michael I Norton, John D Van Horn, Daniel M Wegner, Scott T Grafton, and C Neil Macrae. Wandering minds: the default network and stimulus-independent thought. *Science*, 315(5810):393–395, 2007.

[26] Justin L Vincent, Abraham Z Snyder, Michael D Fox, Benjamin J Shannon, Jessica R Andrews, Marcus E Raichle, and Randy L Buckner. Coherent spontaneous activity identifies a hippocampal-parietal memory network. *Journal of neurophysiology*, 96(6):3517–3531, 2006.

[27] Randy L Buckner, Jessica R Andrews-Hanna, and Daniel L Schacter. The brain's default network. *Annals of the New York Academy of Sciences*, 1124(1):1–38, 2008.

[28] Justin L Vincent, Gaurav H Patel, Michael D Fox, Abraham Z Snyder, Justin T Baker, David C Van Essen, John M Zempel, Lawrence H Snyder, Maurizio Corbetta, and Marcus E Raichle. Intrinsic functional architecture in the anaesthetized monkey brain. *Nature*, 447(7140):83, 2007.

[29] Hanbing Lu, Qihong Zou, Hong Gu, Marcus E Raichle, Elliot A Stein, and Yihong Yang. Rat brains also have a default mode network. *Proceedings of the National Academy of Sciences*, 109(10):3979–3984, 2012.

[30] Silvina G Horovitz, Masaki Fukunaga, Jacco A de Zwart, Peter van Gelderen, Susan C Fulton, Thomas J Balkin, and Jeff H Duyn. Low frequency bold fluctuations during resting wakefulness and light sleep: A simultaneous eeg-fmri study. *Human brain mapping*, 29(6):671–682, 2008.

[31] Michael D Fox and Marcus E Raichle. Spontaneous fluctuations in brain activity observed with functional magnetic resonance imaging. *Nature reviews. Neuroscience*, 8(9):700, 2007.

[32] Michael D Fox, Dongyang Zhang, Abraham Z Snyder, and Marcus E Raichle. The global signal and observed anticorrelated resting state brain networks. *Journal of neurophysiology*, 101(6):3270–3283, 2009.

[33] JS Damoiseaux, SARB Rombouts, F Barkhof, P Scheltens, CJ Stam, Stephen M Smith, and CF Beckmann. Consistent resting-state networks across healthy subjects. *Proceedings of the national academy of sciences*, 103(37):13848–13853, 2006.

[34] Ann S Choe, Craig K Jones, Suresh E Joel, John Muschelli, Visar Belegu, Brian S Caffo, Martin A Lindquist, Peter CM van Zijl, and James J Pekar. Reproducibility and temporal structure in weekly resting-state fmri over a period of 3.5 years. *PloS one*, 10(10):e0140134, 2015.

[35] Christopher M Lewis, Antonello Baldassarre, Giorgia Committeri, Gian Luca Romani, and Maurizio Corbetta. Learning sculpts the spontaneous activity of the resting human brain. *Proceedings of the National Academy of Sciences*, 106(41):17558–17563, 2009.

[36] Damien A Fair, Alexander L Cohen, Nico UF Dosenbach, Jessica A Church, Francis M Miezin, Deanna M Barch, Marcus E Raichle, Steven E Petersen, and Bradley L Schlaggar. The maturing architecture of the brain's default network. *Proceedings of the National Academy of Sciences*, 105(10):4028–4032, 2008.

[37] Michael Greicius. Resting-state functional connectivity in neuropsychiatric disorders. *Current opinion in neurology*, 21(4):424–430, 2008.

[38] Bharat B Biswal, Maarten Mennes, Xi-Nian Zuo, Suril Gohel, Clare Kelly, Steve M Smith, Christian F Beckmann, Jonathan S Adelstein, Randy L Buckner, Stan Colcombe, et al. Toward discovery science of human brain function. *Proceedings of the National Academy of Sciences*, 107(10):4734–4739, 2010.

[39] JS Damoiseaux, CF Beckmann, EJ Arigita, F Barkhof, Ph Scheltens, CJ Stam, SM Smith, and SARB Rombouts. Reduced resting-state brain activity in the âĂIJdefault networkâĂİ in normal aging. *Cerebral cortex*, 18(8):1856–1864, 2008.

[40] Jessica R Andrews-Hanna, Abraham Z Snyder, Justin L Vincent, Cindy Lustig, Denise Head, Marcus E Raichle, and Randy L Buckner. Disruption of large-scale brain systems in advanced aging. *Neuron*, 56(5):924–935, 2007.

[41] Fabio Sambataro, Vishnu P Murty, Joseph H Callicott, Hao-Yang Tan, Saumitra Das, Daniel R Weinberger, and Venkata S Mattay. Age-related alterations in default mode

network: impact on working memory performance. *Neurobiology of aging*, 31(5):839–852, 2010.

[42] Eleni L Vlahou, Franka Thurm, Iris-Tatjana Kolassa, and Winfried Schlee. Resting-state slow wave power, healthy aging and cognitive performance. *Scientific reports*, 4, 2014.

[43] Cheryl L Grady, Andrea B Protzner, Natasa Kovacevic, Stephen C Strother, Babak Afshin-Pour, Magda Wojtowicz, John AE Anderson, Nathan Churchill, and Anthony R McIntosh. A multivariate analysis of age-related differences in default mode and task-positive networks across multiple cognitive domains. *Cerebral cortex*, 20(6):1432–1447, 2010.

[44] Dardo Tomasi and Nora D Volkow. Aging and functional brain networks. *Molecular psychiatry*, 17(5):471, 2012.

[45] Stanislas Dehaene and Lionel Naccache. Towards a cognitive neuroscience of consciousness: basic evidence and a workspace framework. *Cognition*, 79(1):1–37, 2001.

[46] John C Mazziotta, Arthur W Toga, Alan Evans, Peter Fox, and Jack Lancaster. A probabilistic atlas of the human brain: Theory and rationale for its development: The international consortium for brain mapping (icbm). *Neuroimage*, 2(2):89–101, 1995.

[47] John Mazziotta, Arthur Toga, Alan Evans, Peter Fox, Jack Lancaster, Karl Zilles, Roger Woods, Tomas Paus, Gregory Simpson, Bruce Pike, et al. A probabilistic atlas and reference system for the human brain: International consortium for brain mapping (icbm). *Philosophical Transactions of the Royal Society of London B: Biological Sciences*, 356(1412):1293–1322, 2001.

[48] Alan C Evans, Andrew L Janke, D Louis Collins, and Sylvain Baillet. Brain templates and atlases. *Neuroimage*, 62(2):911–922, 2012.

[49] Patric Hagmann, Leila Cammoun, Xavier Gigandet, Reto Meuli, Christopher J Honey, Van J Wedeen, and Olaf Sporns. Mapping the structural core of human cerebral cortex. *PLoS biology*, 6(7):e159, 2008.

[50] Nathalie Tzourio-Mazoyer, Brigitte Landeau, Dimitri Papathanassiou, Fabrice Crivello, Olivier Etard, Nicolas Delcroix, Bernard Mazoyer, and Marc Joliot. Automated anatomical labeling of activations in spm using a macroscopic anatomical parcellation of the mni mri single-subject brain. *Neuroimage*, 15(1):273–289, 2002.

[51] Jörn Diedrichsen, Joshua H Balsters, Jonathan Flavell, Emma Cussans, and Narender Ramnani. A probabilistic mr atlas of the human cerebellum. *Neuroimage*, 46(1):39–46, 2009.

[52] R Cameron Craddock, G Andrew James, Paul E Holtzheimer, Xiaoping P Hu, and Helen S Mayberg. A whole brain fmri atlas generated via spatially constrained spectral clustering. *Human brain mapping*, 33(8):1914–1928, 2012.

[53] Jonathan D Power, Alexander L Cohen, Steven M Nelson, Gagan S Wig, Kelly Anne Barnes, Jessica A Church, Alecia C Vogel, Timothy O Laumann, Fran M Miezin, Bradley L Schlaggar, et al. Functional network organization of the human brain. *Neuron*, 72(4):665–678, 2011.

[54] Susumu Mori and Peter van Zijl. Fiber tracking: principles and strategies–a technical review. *NMR in Biomedicine*, 15(7-8):468–480, 2002.

[55] Patric Hagmann, Leila Cammoun, Xavier Gigandet, Stephan Gerhard, P Ellen Grant, Van Wedeen, Reto Meuli, Jean-Philippe Thiran, Christopher J Honey, and Olaf Sporns. Mr connectomics: principles and challenges. *Journal of neuroscience methods*, 194(1):34–45, 2010.

[56] Michael Breakspear and Viktor Jirsa. Neuronal dynamics and brain connectivity. *Handbook of brain connectivity*, pages 3–64, 2007.

[57] Gustavo Deco, Giulio Tononi, Melanie Boly, and Morten L Kringelbach. Rethinking segregation and integration: contributions of whole-brain modelling. *Nature reviews. Neuroscience*, 16(7):430, 2015.

[58] Gustavo Deco, Adrián Ponce-Alvarez, Patric Hagmann, Gian Luca Romani, Dante Mantini, and Maurizio Corbetta. How local excitation–inhibition ratio impacts the whole brain dynamics. *Journal of Neuroscience*, 34(23):7886–7898, 2014.

[59] Joana Cabral, Etienne Hugues, Olaf Sporns, and Gustavo Deco. Role of local network oscillations in resting-state functional connectivity. *Neuroimage*, 57(1):130–139, 2011.

[60] Gustavo Deco and Viktor K Jirsa. Ongoing cortical activity at rest: criticality, multistability, and ghost attractors. *Journal of Neuroscience*, 32(10):3366–3375, 2012.

[61] Anandamohan Ghosh, Y Rho, Anthony Randal McIntosh, Rolf Kötter, and Viktor K Jirsa. Noise during rest enables the exploration of the brain's dynamic repertoire. *PLoS Comput Biol*, 4(10):e1000196, 2008.

[62] Frank Freyer, James A Roberts, Petra Ritter, and Michael Breakspear. A canonical model of multistability and scale-invariance in biological systems. *PLoS Comput Biol*, 8(8):e1002634, 2012.

[63] Mario Senden, Niels Reuter, Martijn P van den Heuvel, Rainer Goebel, and Gustavo Deco. Cortical rich club regions can organize state-dependent functional network formation by engaging in oscillatory behavior. *NeuroImage*, 2016.

[64] Patricia A Reuter-Lorenz and Katherine A Cappell. Neurocognitive aging and the compensation hypothesis. *Current directions in psychological science*, 17(3):177–182, 2008.

[65] Roberto Cabeza. Hemispheric asymmetry reduction in older adults: the harold model. *Psychology and aging*, 17(1):85, 2002.

[66] Simon W Davis, Nancy A Dennis, Sander M Daselaar, Mathias S Fleck, and Roberto Cabeza. Que pasa? the posterior–anterior shift in aging. *Cerebral cortex*, 18(5):1201–1209, 2007.

[67] Sander M Daselaar, Vijeth Iyengar, Simon W Davis, Karl Eklund, Scott M Hayes, and Roberto E Cabeza. Less wiring, more firing: low-performing older adults compensate for impaired white matter with greater neural activity. *Cerebral cortex*, 25(4):983–990, 2013.

[68] Jie Song, Rasmus M Birn, Mélanie Boly, Timothy B Meier, Veena A Nair, Mary E Meyerand, and Vivek Prabhakaran. Age-related reorganizational changes in modularity and functional connectivity of human brain networks. *Brain connectivity*, 4(9):662–676, 2014.

[69] Cheryl Grady, Saman Sarraf, Cristina Saverino, and Karen Campbell. Age differences in the functional interactions among the default, frontoparietal control, and dorsal attention networks. *Neurobiology of aging*, 41:159–172, 2016.

[70] Gary R Turner and R Nathan Spreng. Prefrontal engagement and reduced default network suppression co-occur and are dynamically coupled in older adults: the default–executive coupling hypothesis of aging. *Journal of cognitive neuroscience*, 2015.

[71] Gwenaëlle Douaud, Adrian R Groves, Christian K Tamnes, Lars Tjelta Westlye, Eugene P Duff, Andreas Engvig, Kristine B Walhovd, Anthony James, Achim Gass, Andreas U Monsch, et al. A common brain network links development, aging, and vulnerability to disease. *Proceedings of the National Academy of Sciences*, 111(49):17648–17653, 2014.

[72] David H Salat, Randy L Buckner, Abraham Z Snyder, Douglas N Greve, Rahul SR Desikan, Evelina Busa, John C Morris, Anders M Dale, and Bruce Fischl. Thinning of the cerebral cortex in aging. *Cerebral cortex*, 14(7):721–730, 2004.

[73] Mario Senden, Niels Reuter, Martijn P van den Heuvel, Rainer Goebel, and Gustavo Deco. Cortical rich club regions can organize state-dependent functional network formation by engaging in oscillatory behavior. *NeuroImage*, 146:561–574, 2017.

[74] Leonardo L Gollo, Andrew Zalesky, R Matthew Hutchison, Martijn van den Heuvel, and Michael Breakspear. Dwelling quietly in the rich club: brain network determinants of slow cortical fluctuations. *Phil. Trans. R. Soc. B*, 370(1668):20140165, 2015.

[75] Linda Geerligs, Mikail Rubinov, Richard N Henson, et al. State and trait components of functional connectivity: individual differences vary with mental state. *Journal of Neuroscience*, 35(41):13949–13961, 2015.

[76] Denise C Park and Patricia Reuter-Lorenz. The adaptive brain: aging and neurocognitive scaffolding. *Annual review of psychology*, 60:173–196, 2009.

[77] Douglas D Garrett, Natasa Kovacevic, Anthony R McIntosh, and Cheryl L Grady. The importance of being variable. *Journal of Neuroscience*, 31(12):4496–4503, 2011.

[78] Cathy J Price and Karl J Friston. Degeneracy and cognitive anatomy. *Trends in cognitive sciences*, 6(10):416–421, 2002.

[79] Arpan Banerjee, Emmanuelle Tognoli, JA Scott Kelso, and Viktor K Jirsa. Spatiotemporal re-organization of large-scale neural assemblies underlies bimanual coordination. *Neuroimage*, 62(3):1582–1592, 2012.

[80] Kai Wu, Yasuyuki Taki, Kazunori Sato, Shigeo Kinomura, Ryoi Goto, Ken Okada, Ryuta Kawashima, Yong He, Alan C Evans, and Hiroshi Fukuda. Age-related changes in topological organization of structural brain networks in healthy individuals. *Human brain mapping*, 33(3):552–568, 2012.

[81] Zhang J Chen, Yong He, Pedro Rosa-Neto, Gaolang Gong, and Alan C Evans. Age-related alterations in the modular organization of structural cortical network by using cortical thickness from mri. *Neuroimage*, 56(1):235–245, 2011.

[82] Tengda Zhao, Miao Cao, Haijing Niu, Xi-Nian Zuo, Alan Evans, Yong He, Qi Dong, and Ni Shu. Age-related changes in the topological organization of the white matter structural connectome across the human lifespan. *Human brain mapping*, 36(10):3777–3792, 2015.

[83] Nico UF Dosenbach, Damien A Fair, Francis M Miezin, Alexander L Cohen, Kristin K Wenger, Ronny AT Dosenbach, Michael D Fox, Abraham Z Snyder, Justin L Vincent, Marcus E Raichle, et al. Distinct brain networks for adaptive and stable task control in humans. *Proceedings of the National Academy of Sciences*, 104(26):11073–11078, 2007.

[84] Michael W Cole and Walter Schneider. The cognitive control network: integrated cortical regions with dissociable functions. *Neuroimage*, 37(1):343–360, 2007.

[85] Cheryl L Grady and Douglas D Garrett. Understanding variability in the bold signal and why it matters for aging. *Brain imaging and behavior*, 8(2):274–283, 2014.

[86] Douglas D Garrett, Natasa Kovacevic, Anthony R McIntosh, and Cheryl L Grady. Blood oxygen level-dependent signal variability is more than just noise. *Journal of Neuroscience*, 30(14):4914–4921, 2010.

[87] Michael Tobia, Mark Meadowcroft, Prasanna Karunanayaka, and Qing Yang. The effects of age on multiscale entropy measurement of neurophysiological signal complexity (1125.6). *The FASEB Journal*, 28(1 Supplement):1125–6, 2014.

[88] R Matthew Hutchison, Thilo Womelsdorf, Elena A Allen, Peter A Bandettini, Vince D Calhoun, Maurizio Corbetta, Stefania Della Penna, Jeff H Duyn, Gary H Glover, Javier Gonzalez-Castillo, et al. Dynamic functional connectivity: promise, issues, and interpretations. *Neuroimage*, 80:360–378, 2013.

[89] Elizabeth N Davison, Benjamin O Turner, Kimberly J Schlesinger, Michael B Miller, Scott T Grafton, Danielle S Bassett, and Jean M Carlson. Individual differences in dynamic functional brain connectivity across the human lifespan. *PLoS computational biology*, 12(11):e1005178, 2016.

[90] Jian Qin, Shan-Guang Chen, Dewen Hu, Ling-Li Zeng, Yi-Ming Fan, Xiao-Ping Chen, and Hui Shen. Predicting individual brain maturity using dynamic functional connectivity. *Frontiers in human neuroscience*, 9:418, 2015.

[91] Demian Battaglia, Boudou Thomas, Enrique CA Hansen, Sabrina Chettouf, Andreas Daffertshofer, Anthony R McIntosh, Joelle Zimmermann, Petra Ritter, and Viktor Jirsa. Functional connectivity dynamics of the resting state across the human adult lifespan. *bioRxiv*, page 107243, 2017.

[92] Kimberly J Schlesinger, Benjamin O Turner, Brian A Lopez, Michael B Miller, and Jean M Carlson. Age-dependent changes in task-based modular organization of the human brain. *NeuroImage*, 146:741–762, 2017.

[93] Fabrizio De Vico Fallani, Jonas Richiardi, Mario Chavez, and Sophie Achard. Graph analysis of functional brain networks: practical issues in translational neuroscience. *Phil. Trans. R. Soc. B*, 369(1653):20130521, 2014.

[94] Mikail Rubinov and Olaf Sporns. Complex network measures of brain connectivity: uses and interpretations. *Neuroimage*, 52(3):1059–1069, 2010.

[95] Vincent D Blondel, Jean-Loup Guillaume, Renaud Lambiotte, and Etienne Lefebvre. Fast unfolding of communities in large networks. *Journal of statistical mechanics: theory and experiment*, 2008(10):P10008, 2008.

[96] Sam Kash Kachigan. *Statistical analysis: An interdisciplinary introduction to univariate & multivariate methods*. Radius Press, 1986.

[97] Linda Geerligs, Natasha M Maurits, Remco J Renken, and Monicque M Lorist. Reduced specificity of functional connectivity in the aging brain during task performance. *Human brain mapping*, 35(1):319–330, 2014.

[98] Patricia A Reuter-Lorenz and Denise C Park. How does it stac up? revisiting the scaffolding theory of aging and cognition. *Neuropsychology review*, 24(3):355–370, 2014.

[99] Peter J Hellyer, Gregory Scott, Murray Shanahan, David J Sharp, and Robert Leech. Cognitive flexibility through metastable neural dynamics is disrupted by damage to the structural connectome. *Journal of Neuroscience*, 35(24):9050–9063, 2015.

[100] Elizabeth L Glisky and Lauren L Kong. Do young and older adults rely on different processes in source memory tasks? a neuropsychological study. *Journal of Experimental Psychology: Learning, Memory, and Cognition*, 34(4):809, 2008.

[101] Enrico Glerean, Juha Salmi, Juha M Lahnakoski, Iiro P Jääskeläinen, and Mikko Sams. Functional magnetic resonance imaging phase synchronization as a measure of dynamic functional connectivity. *Brain connectivity*, 2(2):91–101, 2012.

[102] Mark EJ Newman. Modularity and community structure in networks. *Proceedings of the national academy of sciences*, 103(23):8577–8582, 2006.

[103] Henry Scheffe. A method for judging all contrasts in the analysis of variance. *Biometrika*, pages 87–104, 1953.

[104] Barbara G Tabachnick, Linda S Fidell, and Steven J Osterlind. Using multivariate statistics. 2001.

[105] Makoto Fukushima, Richard F Betzel, Ye He, Marcel A de Reus, Martijn P Heuvel, Xi-Nian Zuo, and Olaf Sporns. Individual variability and connectivity dynamics in modular organization of human cortical functional networks. *arXiv preprint arXiv:1511.06427*, 2015.

[106] Y Yao, WL Lu, B Xu, CB Li, CP Lin, David Waxman, and JF Feng. The increase of the functional entropy of the human brain with age. *Scientific reports*, 3, 2013.

[107] Wolfgang Maass. Networks of spiking neurons: the third generation of neural network models. *Neural networks*, 10(9):1659–1671, 1997.

[108] Changsong Zhou, Lucia Zemanová, Gorka Zamora, Claus C Hilgetag, and Jürgen Kurths. Hierarchical organization unveiled by functional connectivity in complex brain networks. *Physical review letters*, 97(23):238103, 2006.

[109] Christopher J Honey, Rolf Kötter, Michael Breakspear, and Olaf Sporns. Network structure of cerebral cortex shapes functional connectivity on multiple time scales. *Proceedings of the National Academy of Sciences*, 104(24):10240–10245, 2007.

[110] A Ghosh, Y Rho, AR McIntosh, R Kötter, and VK Jirsa. Cortical network dynamics with time delays reveals functional connectivity in the resting brain. *Cognitive neurodynamics*, 2(2):115, 2008.

[111] Joana Cabral, Etienne Hugues, Morten L Kringelbach, and Gustavo Deco. Modeling the outcome of structural disconnection on resting-state functional connectivity. *Neuroimage*, 62(3):1342–1353, 2012.

[112] Gustavo Deco and Morten L Kringelbach. Great expectations: using whole-brain computational connectomics for understanding neuropsychiatric disorders. *Neuron*, 84(5):892–905, 2014.

[113] Anirudh Vattikonda, Bapi Raju Surampudi, Arpan Banerjee, Gustavo Deco, and Dipanjan Roy. Does the regulation of local excitation–inhibition balance aid in recovery of functional connectivity? a computational account. *NeuroImage*, 136:57–67, 2016.

[114] Hermann Haken, JA Scott Kelso, and Heinz Bunz. A theoretical model of phase transitions in human hand movements. *Biological cybernetics*, 51(5):347–356, 1985.

[115] Denis Talay. Numerical solution of stochastic differential equations. 1994.

[116] Karl J Friston, Lee Harrison, and Will Penny. Dynamic causal modelling. *Neuroimage*, 19(4):1273–1302, 2003.

[117] Cheryl Grady. The cognitive neuroscience of ageing. *Nature reviews. Neuroscience*, 13(7):491–505, 2012.

[118] Vince D Calhoun, Robyn Miller, Godfrey Pearlson, and Tulay Adalı. The chronnectome: time-varying connectivity networks as the next frontier in fmri data discovery. *Neuron*, 84(2):262–274, 2014.